JACS
JOURNAL OF THE AMERICAN CHEMICAL SOCIETY
pubs.acs.org/JACS
Article

Reinterpreting the Fate of Iridium(III) Photocatalysts—Screening a Combinatorial Library to Explore Light-Driven Side-Reactions

Joseph C. Bawden, Paul S. Francis,* Stephen DiLuzio, David J. Hayne, Egan H. Doeven, Johnny Truong, Richard Alexander, Luke C. Henderson, Daniel E. Gómez, Massimiliano Massi, Blake I. Armstrong, Felicity A. Draper, Stefan Bernhard,* and Timothy U. Connell*

Cite This: *J. Am. Chem. Soc.* 2022, 144, 11189–11202
Read Online

ABSTRACT: Photoredox catalysts are primarily selected based on ground and excited state properties, but their activity is also intrinsically tied to the nature of their reduced (or oxidized) intermediates. Catalyst reactivity often necessitates an inherent instability, thus these intermediates represent a mechanistic turning point that affords either product formation or side-reactions. In this work, we explore the scope of a previously demonstrated side-reaction that partially saturates one pyridine ring of the ancillary ligand in heteroleptic iridium(III) complexes. Using high-throughput synthesis and screening under photochemical conditions, we identified different chemical pathways, ultimately governed by ligand composition. The ancillary ligand was the key factor that determined photochemical stability. Following photoinitiated electron transfer from a sacrificial tertiary amine, the reduced intermediate of complexes containing 1,10-phenanthroline derivatives exhibited long-term stability. In contrast, complexes containing 2,2′-bipyridines were highly susceptible to hydrogen atom transfer and ancillary ligand modification. Detailed characterization of selected complexes before and after transformation showed differing effects on the ground and excited state reduction potentials dependent on the nature of the cyclometalating ligands and excited states. The implications of catalyst stability and reactivity in chemical synthesis was demonstrated in a model photoredox reaction.

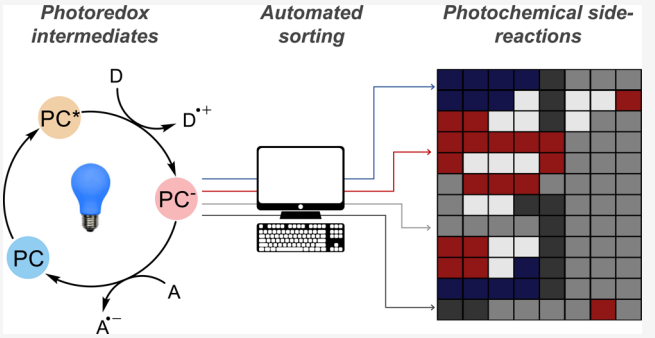

INTRODUCTION

Photoredox catalysis harnesses the energy of visible light to perform otherwise-endergonic electron transfers, as demonstrated in a rapidly expanding array of synthetic applications.[1−7] Most photoredox mechanisms are rationalized by either reductive or oxidative quenching cycles (Figure 1a), comprised of photon absorption and two single electron transfers with substrates, intermediates, and sacrificial electron donors or acceptors. The catalysts that power these light-driven processes (precious or base metal complexes and organic dyes) are generally assumed to be unchanged but, in practice, these materials are rarely recovered or reused. When recovery is attempted, photocatalysts have been found to undergo various side-reactions, often degrading into non-active species.[8−15]

We previously demonstrated that the immediate product of photoinitiated electron transfer (PET) between the common photocatalyst $[Ir(ppy)_2(dtb\text{-}bpy)]^+$ and a tertiary amine [e.g., triethylamine (TEA) or *N*,*N*-diisopropylethylamine (DIPEA)] undergoes subsequent hydrogen atom transfer (HAT), partially reducing the ancillary ligand to the 4,4′-di-*tert*-butyl-1,2,3,4-tetrahydro-2,2′-bipyridine anion ($dtb\text{-}H_3\text{-}bpy^-$; Figure 2a).[16] The transformed neutral complex $[Ir(ppy)_2(dtb\text{-}H_3\text{-}bpy)]^0$ exhibits a large blue shift in emission as well as more reductive ground and excited state potentials. Rather than becoming inactive, tandem reductive and oxidative quenching cycles of $[Ir(ppy)_2(dtb\text{-}bpy)]^+$ and $[Ir(ppy)_2(dtb\text{-}H_3\text{-}bpy)]^0$, respectively, interact to extend the reduction potential window through a multiphoton mechanism (Figure 1b). This cooperative photocatalysis has subsequently enabled the reduction of organohalides[17] and styrene olefins[18] with potentials well beyond the original photocatalyst.

Synthetic methodology utilizing multiphoton excitation (i.e., the input of more than one photon per product output) has grown considerably,[24] driven by a desire to perform demanding reactions with lower photon energies. Common approaches include consecutive photoinduced electron transfer (con-PET; Figure 1c),[19−21] sensitized triplet−triplet annihilation upconversion,[25,26] photoinduced electron transfers with

Received: February 21, 2022
Published: June 15, 2022

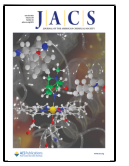

https://doi.org/10.1021/jacs.2c02011
J. Am. Chem. Soc. 2022, 144, 11189−11202

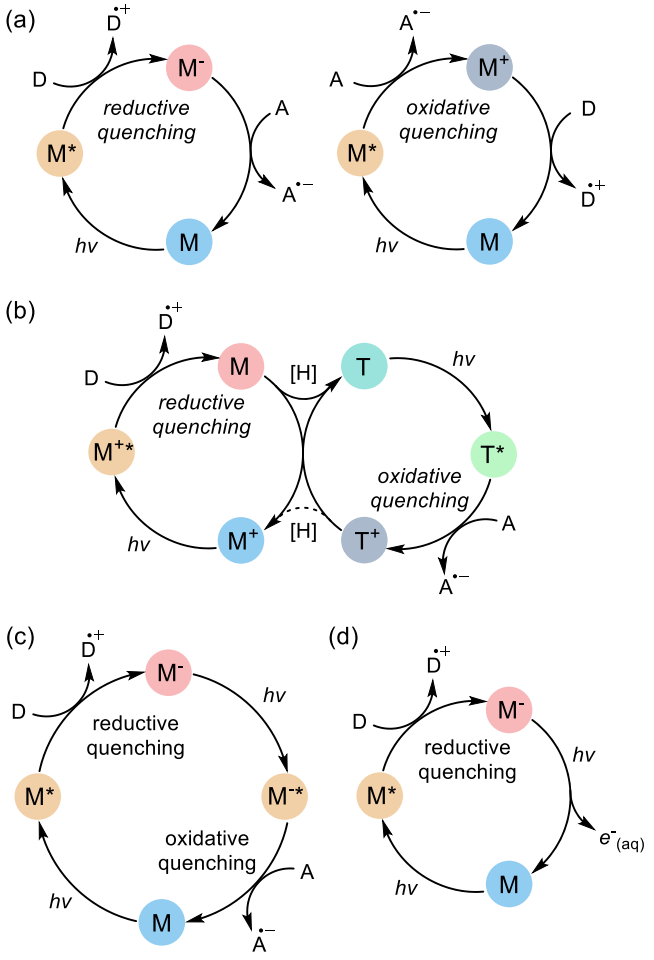

Figure 1. (a) Single-photon photoredox catalysis *via* reductive or oxidative quenching of the catalyst, M, where D is an electron donor and A is an electron acceptor. (b–d) Selected multiphoton cycles, including: (b) the transformation of catalyst, M^+ into a new catalyst, T, enabling a tandem reductive and oxidative photoredox catalysis cycle.[16] (c) consecutive photoinduced electron transfer (con-PET) of catalyst M.[19−21] (d) sequential absorption of two photons by a water-soluble catalyst M to release a hydrated electron.[22,23]

substrates in triplet excited states,[27−29] and sequential two-photon absorption to release a hydrated electron (Figure 1d).[22,30]

Parallel to the development of multi-photon photoredox systems has been the realization that the radical intermediates of sacrificial additives can also extend the driving force of the catalytic cycle.[16,31−37] For example, in addition to acting as hydrogen and electron transfer agents, neutral α-amino alkyl radicals (e.g., $TEA^{\bullet}$; Figure 2b) can facilitate halogen-atom transfer (XAT) for homolytic cleavage of carbon−halogen bonds.[35,36,38]

The greater complexity of multiphoton catalysis requires thorough mechanistic characterization, but often proves difficult to replicate in the controlled environment required for optical spectroscopy. There has been much debate about multiphoton systems,[26,29,41−43] including instances of non-innocent side-products.[19,37,44,45] Pertinent to our study, transient absorption experiments probing the analogous transformation for $[Ir(ppy)_2(bpy)]^+$ with TEA provided evidence that the rate of HAT inversely correlated with the initial amine concentration, likely arising from the competing $TEA^{\bullet+}$ deprotonation pathway by TEA (see Figure 2b).[46] Furthermore, $[Ir(ppy)_2(dtb\text{-}bpy)]^+$ was proposed to generate carbon-centered radicals through a multiphoton con-PET mechanism (primarily demonstrated with organic catalysts;[19−21] Figure 1c) where the critical intermediate $[Ir(ppy)_2(dtb\text{-}bpy^{\bullet-})]^0$ was formed via reductive quenching with ascorbic acid and stabilized in surfactant micelles.[47] Despite rigorous analysis, including the observation that $[Ir(ppy)_2(dtb\text{-}bpy^{\bullet-})]^0$ and the substrate did not react in the absence of light, spectroscopic evidence could not unambiguously distinguish between con-PET, electron expulsion (as elucidated in studies of $[Ru(bpy)_3]^{2+}$ and $[Ir(sppy)_3]^{3-}$; Figure 1d),[22,30] or catalyst transformation (Figure 1b).[48]

Spurred by the recent report of the analogous transformation of $[Ir(ppy)_2(bpy)]^+$ with TEA,[46] and the extensive use of these and related heteroleptic $[Ir(C\text{^}N)_2(N\text{^}N)]^+$ complexes (where C^N is a cyclometalating ligand and N^N is an ancillary diimine ligand) in photoredox catalysis, we suspected this catalyst side-reaction (Figure 2a) may be common and unknowingly contribute to the engagement of energy-demanding substrates. Using combinatorial synthesis and high-throughput screening,[49,50] in conjunction with targeted characterization of select examples, we reveal that under typical photoredox conditions, this chemistry is pervasive for heteroleptic $[Ir(C\text{^}N)_2(N\text{^}N)]^+$ complexes with a 2,2′-bipyridine-type ancillary ligand, while those containing 1,10-phenanthroline derivatives prove resistant to transformation. Where transformation does occur, the effects on the physical properties of the complex vary markedly. These findings recontextualize the role of photocatalysts and their possible side-reactions, while laying the foundation toward a greater understanding of single and multiphoton photoredox catalysis.

RESULTS AND DISCUSSION

High-Throughput Screening. A representative library of 96 cyclometalated iridium(III) complexes was prepared via parallel synthesis,[49,50] in which 12 iridium(III) dimers, differing in the conjugation and electron-withdrawing/donating substituents of their cyclometalating ligands, were combined with eight different polypyridine ancillary ligands (Figure 3a). The resultant complexes exhibited emission colors spanning the visible spectrum and represent a subset of a recent larger study characterizing the heteroleptic $[Ir(C\text{^}N)_2(N\text{^}N)]^+$ excited state composition with respect to relative contributions from ^{3}MLLCT (metal-ligand-to-ligand charge transfer) and ^{3}LC (ligand centered) states.[50] A ^{3}MLLCT excited state (exhibiting characteristic broad, featureless emission bands) corresponds to type I, while type IV signifies ^{3}LC character (typically featuring resolved vibronic peaks in the emission spectra). Intermediate type II and type III complexes represent mixed excited states with greater ^{3}MLLCT or ^{3}LC contributions, respectively. Only complexes containing the 2,2′-biquinoline ancillary ligand resulted in poor luminescence (Figure 3b, Row E), coinciding with the low *in situ* yields reported for these complexes when prepared in dimethylsulfoxide (DMSO).[50]

To explore the scope of the previously observed $[Ir(ppy)_2(dtb\text{-}bpy)]^+$ photocatalyst transformation (Figure 2a),[16] a tertiary amine electron donor was added to the *in situ* prepared complexes and the plate irradiated with blue light in our custom photoreactor (Figure S1). For these experiments,

https://doi.org/10.1021/jacs.2c02011
J. Am. Chem. Soc. 2022, 144, 11189−11202

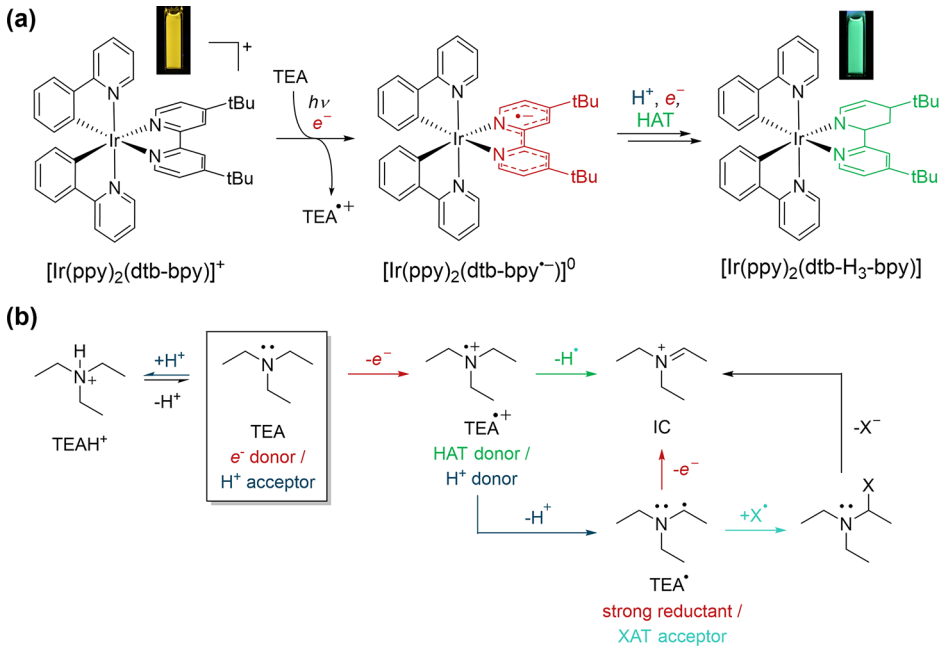

Figure 2. (a) Transformation of the $[Ir(ppy)_2(dtb\text{-}bpy)]^+$ photocatalyst under blue-light irradiation, with a tertiary amine electron donor such as TEA or DIPEA.[16] The transfer to the reduced complex is equivalent to $3H^+$ and $3e^-$ and may involve concerted or stepwise proton and electron transfer and/or hydrogen atom abstraction. The inset photographs show the corresponding change in luminescence color. (b) Selected reactive pathways of TEA,[39,40] including XAT with $TEA^{\bullet}$,[35] and terminating in the iminium cation IC.

triethanolamine (TEOA) was used as the donor, as the volatility of TEA was incompatible with photoreactor conditions. We observed several distinct changes in emission properties, and the screened iridium(III) complexes were qualitatively classified using a custom script (Figure 4a–c). First, complexes with no significant change in emission color or intensity (<±15% relative to a control plate without TEOA) indicated no interaction between the excited state and quencher. Second, we grouped complexes that underwent a significant decrease in emission intensity (>35% during irradiation). Finally, the remaining complexes exhibited an increase in emission intensity during irradiation and were sorted based on their change in emission color. We assigned an emission blue shift or red shift if the color value ("hue" from HSB color space) shifted three relative standard deviations above or below the uniform mean, or no color change if within this confidence interval. This analysis sorted the library of iridium(III) complexes into five groups: no interaction (1), decreased emission intensity (2), or increased emission intensity along with a blue shift (3), red shift (4), or no change (5) in emission color (Figure 4c).

Remarkably, a change in emission color, similar to our original observation with $[Ir(ppy)_2(dtb\text{-}bpy)]^+$, was pervasive throughout complexes containing 2,2′-bipyridine-type ancillary ligands (rows A–D), although those containing 4,4′-diphenyl-2,2′-bipyridine (row D) changed slower than the less-conjugated congeners (Figure S2). In contrast, complexes containing 1,10-phenanthroline or its derivatives (rows F–H) almost exclusively decreased in intensity, and only a handful of wells revealed any visible emission after photoreaction (Figure 4b). The emission intensity from complexes containing 4,7-dimethyl-1,10-phenanthroline (row G, Figure S3) typically decreased at a slower rate than other phenanthroline derivatives (rows H and F).

Although the complexes containing 1,10-phenanthroline-type ancillary ligands decreased in emission intensity irrespective of type I–IV classification (Figure 4d–f), the photochemistry of complexes containing 2,2′-bipyridines was influenced by their excited state morphology. Emission blue shifts (group 3) were more commonly recorded in complexes with type I excited states, while type III/IV excited states preferentially recorded red-shifted emission (group 4) or no color change (group 5, Figure 4g–i). While these trends are noteworthy, excited state morphology is clearly not the only factor that governs photocatalyst fate; plate-wide results showed that each excited state morphology (type I–IV) contains at least one example of each photochemical response (group 1–5).

Select members of each group (green highlights in Figures 3b and 4a–c) were prepared *via* batch synthesis to better understand this varied photochemistry. We chose $[Ir(piq)_2(dm\text{-}bpy)]^+$ (plate position A12) for group 1 and the archetypal $[Ir(ppy)_2(phen)]^+$ (H1) for group 2 (which predominantly comprised complexes with 1,10-phenanthroline derivatives). Complexes with blue-shifted emission (group 3) mainly comprised substituted 2-phenylpyridine cyclometalating ligands, and we selected $[Ir(ppy)_2(dm\text{-}bpy)]^+$ and $[Ir(df\text{-}ppy)_2(dm\text{-}bpy)]^+$ in addition to the previously examined $[Ir(ppy)_2(dtb\text{-}bpy)]^+$ complex (A1, A2, and B1, respectively). The commonly used photoredox catalysts $[Ir(df(CF_3)\text{-}ppy)_2(dtb\text{-}bpy)]^+$ and $[Ir(df(CF_3)ppy)_2(bpy)]^+$ (B3 and C3) were chosen as representatives of groups 4 and 5, respectively, with $[Ir(bt)_2(dm\text{-}bpy)]^+$ (A4) as an additional member of group 4 exhibiting low-energy emission.

Spectroscopic Interrogation. We examined the absorption and emission of the selected complexes under photochemical conditions (photocatalyst, TEA, degassed with Ar, blue LEDs) using a previously described closed-loop flow system (Figure S4).[16] Emission spectra (Figures 5, S5) in the

https://doi.org/10.1021/jacs.2c02011
J. Am. Chem. Soc. 2022, 144, 11189–11202

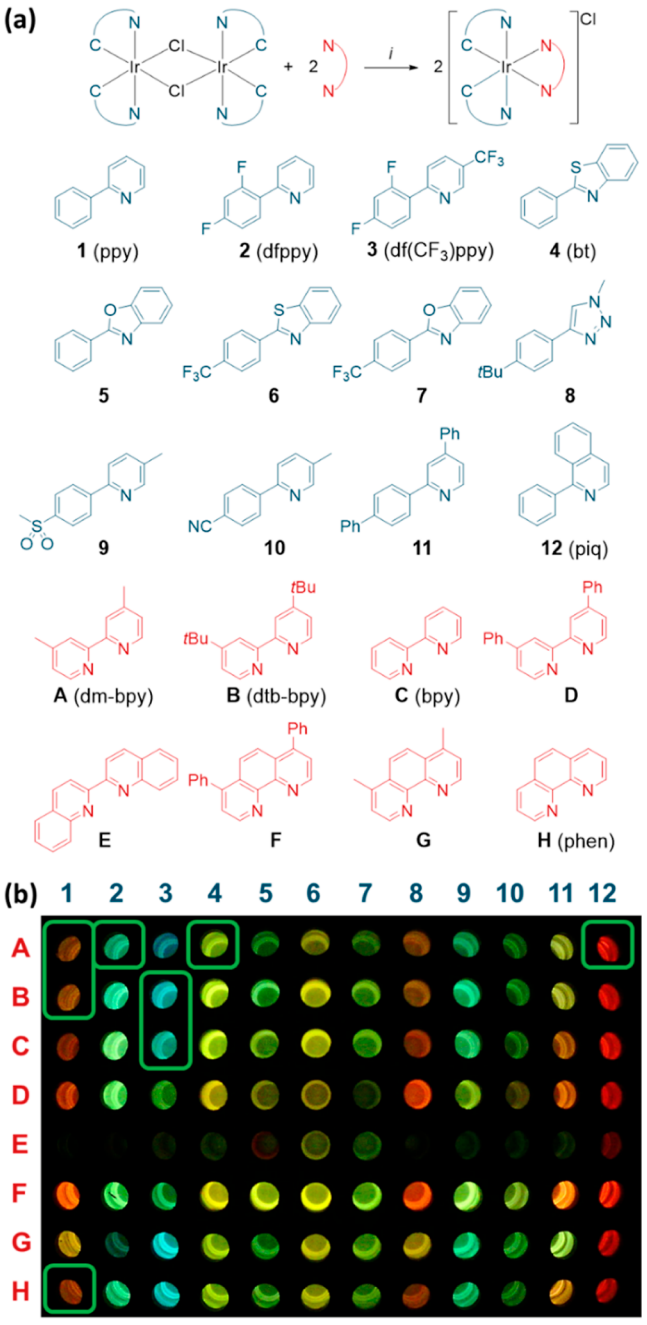

Figure 3. (a) *In situ* iridium(III) complex synthesis and the cyclometalating (blue) and ancillary ligands (red) used to prepare the combinatorial library. Reaction conditions (i) DMSO, 150 °C, 16 h. (b) Luminescence of the synthesized library, imaged in the photoreactor. Complexes selected for subsequent characterization are highlighted in green.

absence of a quencher matched the relative intensities and colors observed during screening. Luminescence quenching with a sacrificial tertiary amine electron donor generally increased with the excited state reduction potential ($M^{+*/0}$) of the photocatalyst (Table S1; vide infra), ranging from no quenching of $[Ir(piq)_2(dm\text{-}bpy)]^+$ to ≥97% for the three complexes with fluorinated cyclometalating ligands. After irradiating for 10 min, most complexes exhibited changes in emission intensity and color consistent with the high-throughput screening (Tables 1 and 2). We detected no change in the emission for $[Ir(piq)_2(dm\text{-}bpy)]^+$ (group 1) and a total disappearance of $[Ir(ppy)_2(phen)]^+$ emission (group 2, Figure 5b). In contrast, all group 3 complexes exhibited an emission blue shift (Figures 5a, S5) consistent with the transformation previously reported for $[Ir(ppy)_2(dtb\text{-}bpy)]^+$ and $[Ir(ppy)_2(bpy)]^+$,[16,46] where the initial broad structureless emission (type I excited state) was replaced by a new peak with vibronic substructure (type III/IV excited state; Figure S5). A red shift in emission was observed for both group 4 complexes and, surprisingly, also the group 5 complex (Figure S5). The emission of $[Ir(bt)_2(dm\text{-}bpy)]^+$ underwent only a subtle change (~9 nm) and retained a type III/IV excited state spectral profile. Both $[Ir(df(CF_3)ppy)_2(dtb\text{-}bpy)]^+$ and $[Ir(df(CF_3)ppy)_2(bpy)]^+$ exhibited a large red shift (~40 nm) to a broader, less-structured band that suggests a more ^{3}MLLCT dominated excited state (type II) is formed (Figure S6). The inaccurate plate classification of $[Ir(df(CF_3)ppy)_2(bpy)]^+$ to group 5 likely results from a much slower transformation rate; this complex exhibited an initial decrease in emission intensity that persisted for ~6 min before a slow red shift (>20 min irradiation) to a new peak.

Substituting the tertiary amine TEA (E^0 = 0.95 V vs SCE[58]) for the alternative electron donor tetra-*n*-butylammonium oxalate (TBAOX), which is oxidized at lower potential (E^0 = 0.06 V *vs* SCE[59]), strongly quenched the emission from all eight iridium(III) complexes ($[Ir(piq)_2(dm\text{-}bpy)]^+$ by 75% and the others by ≥ 95%; Table S1) and afforded no change in emission color upon prolonged irradiation. Unlike TEA, TBAOX cannot act as a proton or hydrogen-atom donor and instead leads to a buildup of the reduced intermediate, which in the case of $[Ir(ppy)_2(dtb\text{-}bpy^{\bullet-})]^0$ is readily characterized by two intense absorbance peaks between 430 and 550 nm and a broader band extending beyond 800 nm.[16,47,60] Similar absorption features emerged for all complexes with 2,2′-bipyridine derivatives as the ancillary ligand (Figure S7, black plots), supporting the formation of analogous reduced intermediates following PET with TBAOX. Only the PET product of $[Ir(ppy)_2(phen)]^+$ and TBAOX exhibited a different absorption profile, with a broad structureless band spanning the entire visible region (Figure 5d, black plot) that we assigned to $[Ir(ppy)_2(phen^{\bullet-})]^0$. Absorption spectra of complexes reduced electrochemically (*via* bulk electrolysis) matched the photochemical reduction products (Figure S7, red plots).

When using TEA as the electron donor, only the $[Ir(ppy)_2(phen)]^+$ complex (group 2) exhibited a similar accumulation of the reduced intermediate (Figure 5d,f). The group 1 complex $[Ir(piq)_2(dm\text{-}bpy)]^+$ did not interact with this quencher, while for complexes in groups 3−4, the characteristic absorption bands of the reduced intermediate were transiently observed and their depletion mirrored by the emergence of the new emissive species (Figures 5e, S8; blue plots). This is consistent with our previous observations[16] that changing emission color results from further reactivity of the initial PET photoproduct and that HAT is an intrinsic step of this side-reaction. Further experiments also suggest the lability of hydrogens is important for catalyst transformation; irradiation of $[Ir(ppy)_2(dtb\text{-}bpy)]^+$ in the presence of TBAOX (electron source) and allyl benzoate (hydrogen source) did not afford significant transformation in comparison with TEA (Figure S9).

Given the similar photochemical response of complexes containing 1,10-phenanthrolines in screening, and the intense color of the reduced intermediates (Figures 5c,d, S10), we

https://doi.org/10.1021/jacs.2c02011
J. Am. Chem. Soc. 2022, 144, 11189−11202

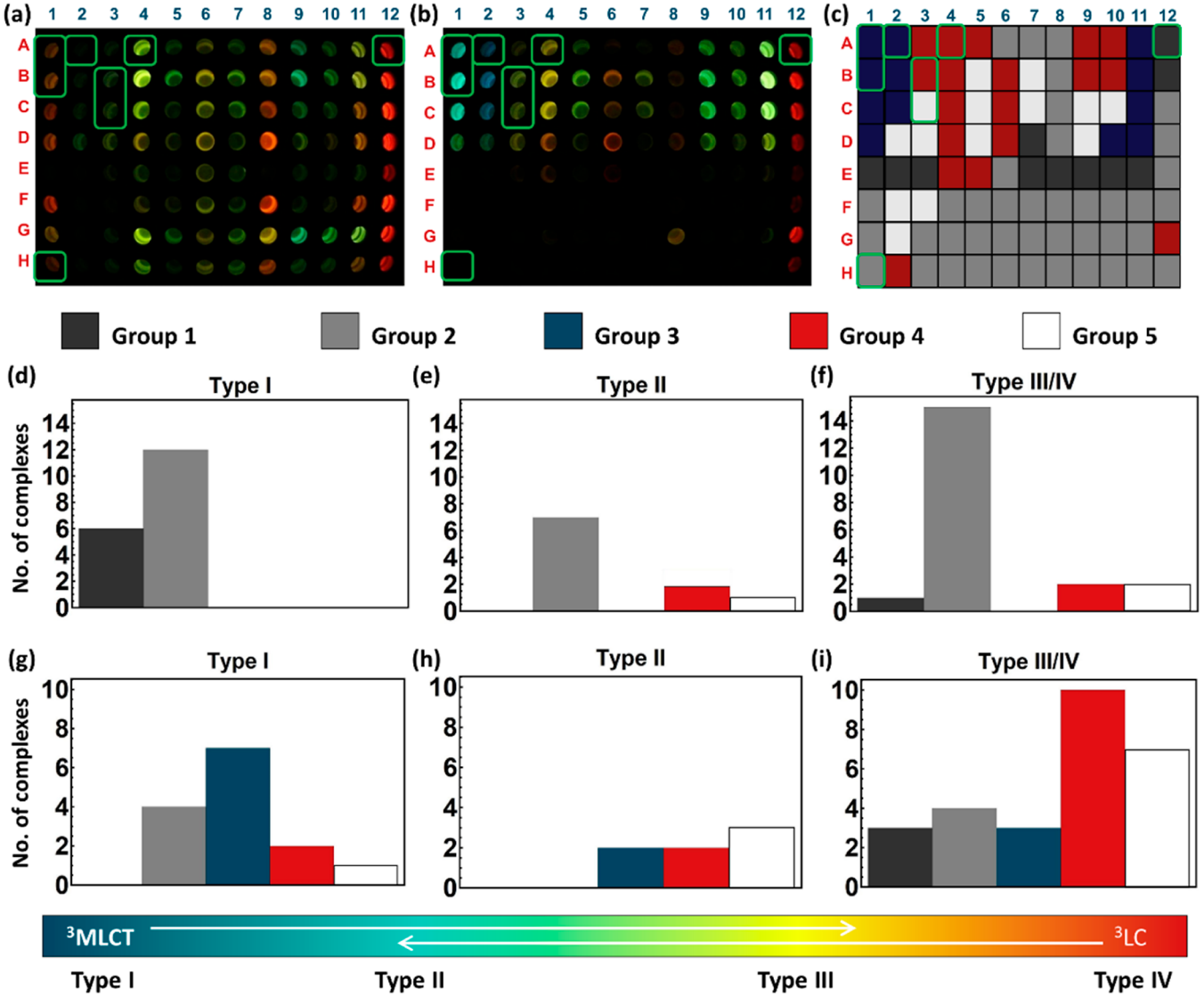

Figure 4. Photographs (a) before and (b) after irradiation of combinatorial library and TEOA. (c) Screening results were sorted into five groups using a custom Python script: group 1—no interaction; group 2—decreased emission intensity; group 3—emission color blue shift; group 4—emission color red shift, and group 5—increased emission intensity but no color change. Complexes selected for subsequent characterization are highlighted in green. Histograms plotting sorted screening results relative to excited state morphology (type I–IV) of (d–f) 1,10-phenanthrolines and 2,2′-biquinoline and (g–i) 2,2′-bipyridines. Type I and type IV excited states are assigned as pure ^{3}MLLCT and ^{3}LC excited states, respectively, while type II and type III represent mixed triplet states with greater MLLCT or LC contributions, respectively.

were curious to explore the stability of the reduced intermediate across the screening library. We repeated the high-throughput photochemical screening using a broadband white LED (3000–3500 K) for imaging. All complexes initially appeared slightly yellow (Figure S11a) and, with irradiation, most 1,10-phenanthroline derivatives (rows F–H) underwent a persistent color change visible to the naked eye (Figure S11b) consistent with the reduced intermediate. Persistent, strongly absorbing intermediates, indicative of a group 2 photo-response, were also observed in several phenanthroline-containing complexes previously categorized as group 4 or 5 (Figures 4c, S11). We attribute this limited accuracy in plate classification to significant emission quenching by the tertiary amine prior to irradiation. Formation of strongly absorbing reduced intermediates was readily monitored using the normalized saturation (white-to-color, HSB color space) of the digitized data, which also revealed a transient change in complexes with 2,2′-bipyridine-type ancillary ligands (rows A–D, Figure S12). The sharp rise in saturation when irradiated (i.e., reduced intermediate formation), followed by either a persistence or decay of signal in 1,10-phenanthrolines (rows F–H) or 2,2′-bipyridines (rows A–D), respectively, matched our spectroscopic observations (Figure 5e,f). Fitted analysis of the decay in complexes with 2,2′-bipyridine-type ligands revealed the reduced intermediate was more long-lived in complexes containing 4,4′-diphenyl-2,2′-bipyridine (row D, Figure S12b, Table S2), consistent with the slower concomitant change in emission color (Figure S2). Fitting of the initial rise also confirmed our previous observation that complexes containing 4,7-dimethyl-1,10-phenanthroline (row G) reduced at a slower rate than other ancillary ligands (Table S2). Interestingly, several complexes containing 2,2′-biquinoline ligands (row E) classified as group 1 also exhibited a persistent color change, indicating similar photochemistry to the 1,10-phenanthroline complexes despite poor *in situ* complexation.

https://doi.org/10.1021/jacs.2c02011
J. Am. Chem. Soc. 2022, 144, 11189–11202

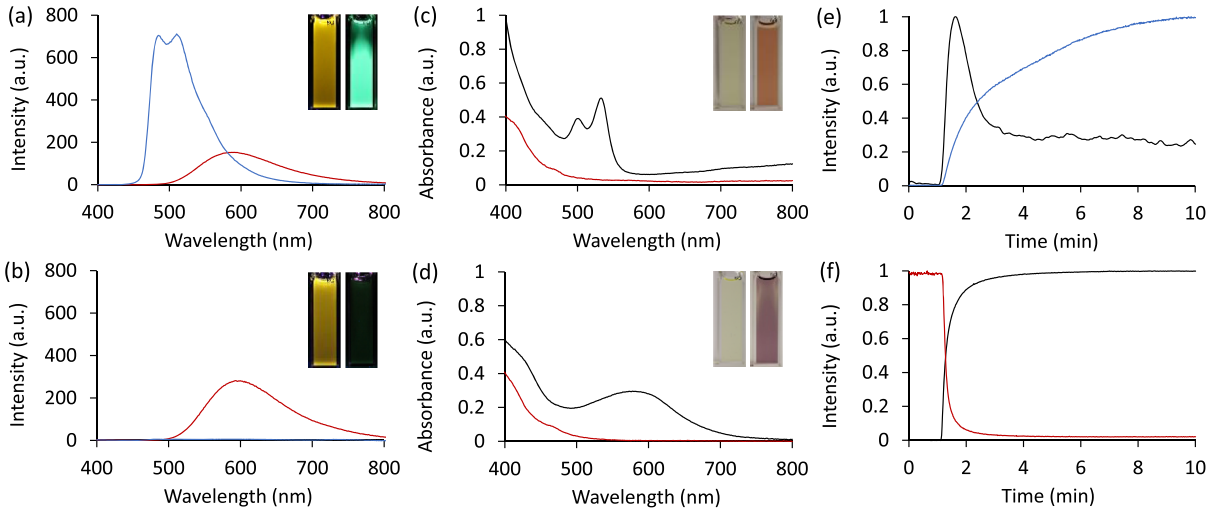

Figure 5. Luminescence spectra of (a) $[Ir(ppy)_2(dtb\text{-}bpy)]^+$ or (b) $[Ir(ppy)_2(phen)]^+$, before (red plots) and after (blue plots) irradiation with blue light using TEA as an electron donor. Inset photographs: emission color before (left) and after (right) irradiation. Absorption spectra of (c) $[Ir(ppy)_2(dtb\text{-}bpy)]^+$ or (d) $[Ir(ppy)_2(phen)]^+$, before (red plots) and after (black plots) irradiation with blue light using TBAOX as an electron donor. Inset photographs: solution color before (left) and after (right) irradiation. (e) Monitoring the transformation of $[Ir(ppy)_2(dtb\text{-}bpy)]^+$ during irradiation with blue light using TEA as an electron donor, through the absorbance of $[Ir(ppy)_2(dtb\text{-}bpy^{\bullet-})]^0$ (black plot), and emission of $[Ir(ppy)_2(dtb\text{-}H_3\text{-}bpy)]^0$ (blue plot). (f) Monitoring the reduction of $[Ir(ppy)_2(phen)]^+$ during irradiation with blue light using TEA as an electron donor, through the emission of $[Ir(ppy)_2(phen)]^+$ (red plot) and absorbance of $[Ir(ppy)_2(phen^{\bullet-})]^0$ (black plot), Absorbance and emission intensities in (e,f) have been normalized.

Table 1. Selected Spectroscopic and Electrochemical Properties for the Iridium(III) Complexes

	emission, λ_{max} (nm)			ground state potentials (V *vs* SCE)			excited state potentials (V *vs* SCE)	
complex	r.t.[a,b]	85 K[b,c]	E_{0-0} (eV)[d]	$E^{0\prime}(M^{+/0})$	$E^{0\prime}(M^{2+/+})$	ΔE	$E^0(M^{+*/0})$[e]	$E^0(M^{2+/+*})$[f]
$[Ir(piq)_2(dm\text{-}bpy)]^+$ (A12)	597	581	2.13	−1.46	1.23	2.69	0.68	−0.90
$[Ir(ppy)_2(phen)]^+$ (H1)	595	508	2.44	−1.36	1.27	2.63	1.08	−1.17
$[Ir(ppy)_2(dtb\text{-}bpy)]^+$ (B1)	590	473	2.4[g]	−1.48	1.25	2.72	0.92	−1.15
$[Ir(ppy)_2(dm\text{-}bpy)]^+$ (A1)	589	509	2.44	−1.46	1.25	2.71	0.98	−1.19
$[Ir(df\text{-}ppy)_2(dm\text{-}bpy)]^+$ (A2)	521	450	2.76	−1.40	1.57	2.97	1.36	−1.18
$[Ir(bt)_2(dm\text{-}bpy)]^+$ (A4)	526	515	2.41	−1.43	1.40	2.82	0.98	−1.01
$[Ir(df(CF_3)ppy)_2(dtb\text{-}bpy)]^+$ (B3)	475	463	2.68	−1.34	1.73	3.07	1.34	−0.95
$[Ir(df(CF_3)ppy)_2(bpy)]^+$ (C3)	475	462	2.68	−1.25	1.74	2.99	1.43	−0.94

[a]Metal complexes at 10 μM in acetonitrile at ambient temperature. [b]Corrected for the change in instrument sensitivity over the wavelength range. [c]Metal complexes at 5 μM in 4:1 EtOH/MeOH at 85 K. [d]Energy between the zeroth vibrational levels of the ground and excited states, estimated from the highest energy band of the low-temperature emission spectrum, unless otherwise indicated. [e]Estimated using $E^0(M^{+*/0}) = E^{0\prime}(M^{+/0}) + E_{0-0}$. [f]Estimated using $E^0(M^{2+/+*}) = E^{0\prime}(M^{2+/+}) - E_{0\text{-}0}$. [g]Commonly reported potentials for the excited state of $[Ir(ppy)_2(dtb\text{-}bpy)]^+$ were established using a first approximation of E_{0-0} (2.17 eV) from the spectral distribution at ambient temperature.[51] Subsequent estimation (2.62 eV) based on the emission at 77 K,[52] however, may be an overestimate, due to the contribution of higher energy transitions.[53−55] Our estimate of ∼2.4 eV was based on spectra under multiple conditions[16] and values obtained for related complexes.[56,57]

What is the Transformed Photoproduct? In our previous work identifying the transformed complex $[Ir(ppy)_2(dtb\text{-}H_3\text{-}bpy)]^0$, we proposed the partial saturation of the ancillary ligand (Figure 2a) supported by extensive structural characterization.[16] Our more recent attempts to isolate $[Ir(ppy)_2(dtb\text{-}H_3\text{-}bpy)]^0$ by column chromatography, however, were impeded by the incomplete conversion under preparative scale conditions, the presence of isomers (likely due to different saturation geometry of the transformed pyridine ring), and further product degradation with longer irradiation. Nevertheless, the ^{1}H NMR spectroscopy of the transformation product obtained under these conditions (Figure S13) is consistent with our original proposal.

Electrospray ionization-mass spectrometry (ESI-MS) of an irradiated solution of $[Ir(ppy)_2(dtb\text{-}bpy)]^+$ (m/z 769.287, Figure 6a) and TEA evolved two major iridium species with mass differences of +4 and +103 (Figure 6b). Using high-resolution spectra, we assigned these as two different ionization states of the same neutral complex; $[[Ir(ppy)_2(dtb\text{-}H_3\text{-}bpy)]+H]^+$ (m/z 773.318) and $[[Ir(ppy)_2(dtb\text{-}H_3\text{-}bpy)]+IC]^+$ (m/z 872.424), where IC is the iminium cation photoproduct following oxidation of TEA (Figure 2b). Tandem MS/MS experiments also confirmed that structural changes occur exclusively on the ancillary ligand rather than the iridium(III) cyclometalated core.[16] When comparing the photochemistry of $[Ir(ppy)_2(dtb\text{-}bpy)]^+$ with our selected photocatalysts, group 1 and 2 complexes ($[Ir(piq)_2(dm\text{-}bpy)]^+$ and $[Ir(ppy)_2(phen)]^+$, respectively) showed no evidence of transformation even after prolonged irradiation (Figure S14). All group 3−4 complexes exhibited mass spectra with a similar distribution of iridium(III) species to our previous experiments (Figures 6, S14−S15). Using $[Ir(ppy)_2(dm\text{-}bpy)]^+$ (m/z

https://doi.org/10.1021/jacs.2c02011
J. Am. Chem. Soc. 2022, 144, 11189−11202

Table 2. Selected Spectroscopic and Electrochemical Properties for the New Species Generated by Irradiation of the Precursor Iridium(III) Complex under Photochemical Conditions

	emission, λ_{max} (nm)			ground state potentials (V *vs* SCE)			excited state potentials (V *vs* SCE)	
precursor	r.t.[a,b]	85 K[b,c]	E_{0-0} (eV)[d]	$E^{0\prime}(T^{0/-})$	$E^{(i)}(T^{+/0})$[e]	ΔE (V)	$E^0(T^{0*/-})$[f]	$E^0(T^{+/0*})$[g]
$[Ir(ppy)_2(dtb\text{-}bpy)]^+$ (B1)	485	482	2.57	−1.96	0.88[h]	2.87	0.61	−1.69
$[Ir(ppy)_2(dm\text{-}bpy)]^+$ (A1)	489	483	2.57	−1.94	0.86	2.80	0.63	−1.71
$[Ir(df\text{-}ppy)_2(dm\text{-}bpy)]^+$ (A2)	459	453	2.74	−1.80	1.22	3.02	0.94	−1.52
$[Ir(bt)_2(dm\text{-}bpy)]^+$ (A4)	535	516	2.40	−1.62	0.94	2.56	0.78	−1.46
$[Ir(df(CF_3)ppy)_2(dtb\text{-}bpy)]^+$ (B3)	519	477	2.60	−1.52	(1.44)[i]	2.96	1.08	−1.16
				−1.87	1.07	2.94	0.73	−1.53
$[Ir(df(CF_3)ppy)_2(bpy)]^+$ (C3)	553	471	2.63	−1.49	1.44	2.93	1.14	−1.19
				−1.92	1.01	2.93	0.71	−1.62

[a]From spectra obtained after 10 min irradiation of the metal complex and TEA in the flow system (Figures S4 and S5). [b]Corrected for the change in instrument sensitivity over the wavelength range. [c]Complexes transformed in acetonitrile, then diluted with 4:1 EtOH/MeOH and cooled to 85 K. [d]Energy between the zeroth vibrational levels of the ground and excited states, estimated from the highest energy band of the low-temperature emission spectrum. [e]Inflection point of the anodic wave. [f]Estimated using $E^0(T^{0*/-}) = E^{0\prime}(T^{0/-}) + E_{0-0}$. [g]Estimated using $E^0(T^{+/0*}) = E^{(i)}(T^{+/0}) - E_{0-0}$. [h]The measured $E^{(i)}$ of this species (0.98 V vs SCE) was influenced by a close peak of the remaining parent complex. We have therefore used our previous estimate of the potential derived from the voltametric onset of electrochemiluminescence,[16] which is similar to $E^{(i)}$ of the transformation product of $[Ir(ppy)_2(dm\text{-}bpy)]^+$. [i]Obscured by adjoining peaks; estimate based on the peak of the analogous product of $[Ir(df(CF_3)ppy)_2(bpy)]^+$.

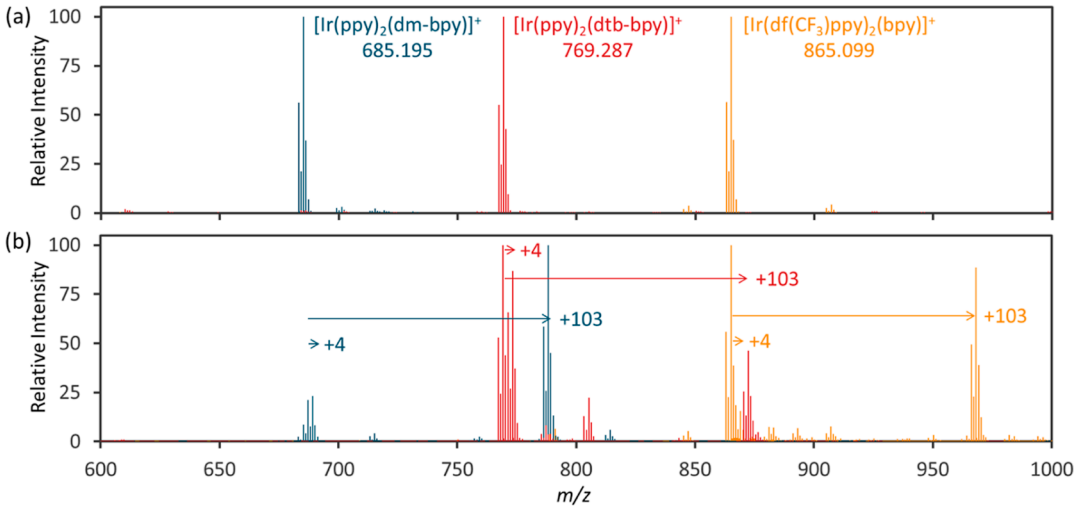

Figure 6. Overlaid ESI mass spectra of $[Ir(ppy)_2(dm\text{-}bpy)]^+$ (blue), $[Ir(ppy)_2(dtb\text{-}bpy)]^+$ (red), and $[Ir(df(CF_3)ppy)_2(bpy)]^+$ (orange) (a) before and (b) after irradiation in presence of a tertiary alkylamine electron donor. The same mass difference was observed in all transformed complexes.

685.195) as an example (Figure 6, blue plot), the same +4 (*m*/*z* 689.225) and +103 (*m*/*z* 788.331) peaks are present with the characteristic iridium isotope pattern. The dication assigned to the transformed metal complex with both a proton and IC associated was also observed in the spectra for several complexes (Figure S14).

Spectra obtained after prolonged irradiation usually afforded no other identifiable products, although further degradation, with the appearance of many small unidentifiable peaks, was not uncommon. An exception was an additional major species appearing for both $[Ir(df(CF_3)ppy)_2(bpy)]^+$ and $[Ir(df(CF_3)\text{-}ppy)_2(dtb\text{-}bpy)]^+$ (Figure S15). For $[Ir(df(CF_3)ppy)_2(bpy)]^+$ (*m*/*z* 865.099), this third species appeared at +206 mass units (*m*/*z* 1071.372) above the parent compound, which we assigned to the complex cation $[[Ir(df(CF_3)ppy)_2(H_6\text{-}bpy)]+2IC]^+$ featuring analogous saturation of the ancillary ligand's remaining pyridyl ring. This negatively charged iridium(III) complex only appears in the positive mode with two equivalents of the IC iminium cation. Comparing the tandem MS/MS fragmentation of all $[Ir(df(CF_3)ppy)_2(bpy)]^+$ transformed species with those of $[Ir(ppy)_2(dtb\text{-}H_3\text{-}bpy)]^0$ revealed the same fragmentation pathways (Figure S16); ready loss of the IC cation (*m*/*z* 100) followed by the transformed ancillary ligand, yielding the cyclometalated core $[Ir(C^\wedge N)_2]^+$ as collision energy increased.

Ground and Excited State Potentials. The ground state electrochemical potentials of the iridium(III) complexes (Table 1) were in good agreement with previously reported values (Table S1, Figure S17).[51,52,56,61−63] Reduction potentials ($T^{0/-}$) of the transformed complexes (group 3−4) were collected by sequential cyclic voltammetry after repeated irradiation of the complex in the presence of TEA and electrolyte (Figures S18 and S19). Following transformation, the complexes exhibited new quasireversible peaks with potentials ranging 0.18−0.48 V below the original complex (Table 2, Figures 7, S18). The cyclic voltammogram of the group 1 complex $[Ir(piq)_2(dm\text{-}bpy)]^+$ was unaffected by irradiation, while the first peak of the group 2 complex $[Ir(ppy)_2(phen)]^+$ disappeared, consistent with the stable reduction product formed photochemically (*vide supra*). Under

https://doi.org/10.1021/jacs.2c02011
J. Am. Chem. Soc. 2022, 144, 11189−11202

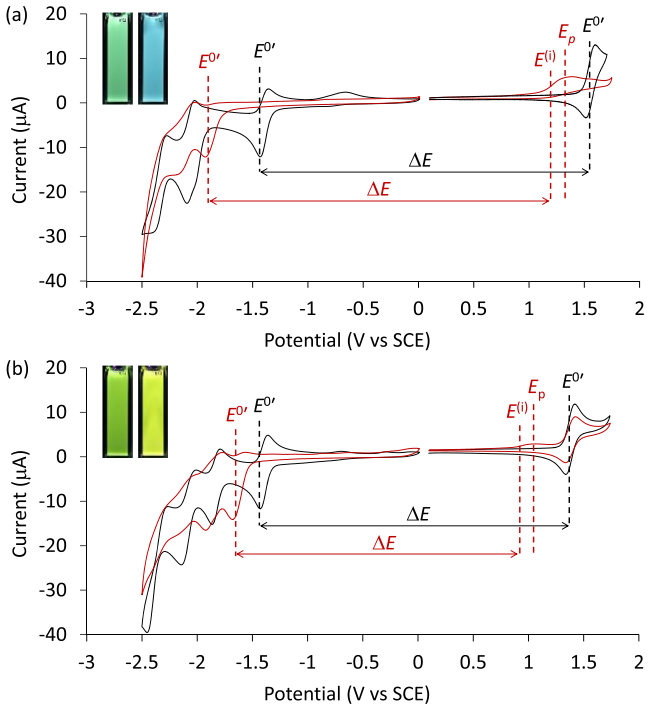

Figure 7. Cyclic voltammograms for (a) $[Ir(df\text{-}ppy)_2(dm\text{-}bpy)]^+$ and (b) $[Ir(bt)_2(dm\text{-}bpy)]^+$ before (black plots) and after (red plots) irradiation with blue light in the presence of TEA. The voltammograms at positive potentials were obtained after the removal of remaining TEA and its photoreaction products. Inset photographs: emission color before (left) and after (right) irradiation.

these conditions, the oxidation of the complexes ($M^{2+/+}$; $T^{+/0}$) was obscured by excess TEA and associated photoproducts. We therefore performed cyclic and square-wave voltammetry on extracted complexes washed with aqueous acetic acid to remove these interferences (Figures 7, S20). The group 1 and 2 complexes showed no change in these experiments, while each group 3−4 complex revealed a new irreversible peak at potentials 0.2−0.4 V lower than that of the original complex (Table 2). We estimated the standard potentials (E^0) using the inflection point of the anodic wave ($E^{(i)}$), which provides a closer approximation than the peak potential (E_p).[64]

The square-wave voltammogram for the transformed $[Ir(df(CF_3)ppy)_2(bpy)]^+$ complex showed two new anodic peaks (Figure S20g) that exhibited the same potential gap (ΔE; Table 2) with reduction peaks ($T^{0/-}$) that were more prominent at different irradiation times (Figures S18 and S19). These distinct species likely arise from the sequential saturation of the two pyridyl rings of the ancillary ligand (i.e., $[Ir(df(CF_3)ppy)_2(H_3\text{-}bpy)]^0$ and $[Ir(df(CF_3)ppy)_2(H_6\text{-}bpy)]^-$) observed by MS. The electrochemical properties for the transformed $[Ir(df(CF_3)ppy)_2(dtb\text{-}bpy)]^+$ complex were similar, except that no maximum was observed at ∼1.4 V, likely due to the broad adjoining peaks and different transformation rates than those of $[Ir(df(CF_3)ppy)_2(bpy)]^+$.

In general, transformation of complexes in group 3 (e.g., $[Ir(df\text{-}ppy)_2(dm\text{-}bpy)]^+$; Figure 7a) elicited a greater change in the potential of their reduction ($M^{+/0}$) than their oxidation ($M^{2+/+}$) (increase in ΔE; c.f. Tables 1 and 2). These changes represent greater destabilization of the LUMO than the HOMO, in line with the observed emission blue shift (e.g., Figure 7a, inset photographs). Conversely, transformation of complexes in group 4 (e.g., $[Ir(bt)_2(dm\text{-}bpy)]^+$; Figure 7b) resulted in a greater change in the potential of their oxidation ($M^{2+/+}$) than their reduction ($M^{+/0}$) (decrease in ΔE), representing greater destabilization of the HOMO than LUMO, corresponding to the observed emission red shift.

The excited state potentials of the iridium(III) complexes (Table 1) and their transformation products (Table 2) were estimated using the difference in energy between the zeroth vibrational levels of the ground and excited states (E_{0-0}), approximated from low-temperature emission spectra (Figure S21). Compared to the ground state potentials, larger disparities exist in reported excited state potentials, predominantly due to the different approaches employed to estimate E_{0-0} (Table S3), but our values matched those reported using similar methods.[62,63]

Despite the large shift in the room-temperature emission λ_{max} upon the photoinitiated transformation of the complex with TEA, we saw only small changes in E_{0-0}. The resulting estimations of the excited state potentials (Table 2) indicate that the transformation of group 3 complexes can extend the reduction strength by 0.12−0.25 V ($T^{+/0*}$ *vs* $M^{+/0}$) under conditions that permit a tandem photoredox catalysis mechanism (Figure 1d). The transformation of complexes in group 4, however, is more complicated and not necessarily advantageous; a tandem photoredox cycle utilizing these complexes would offer negligible change or even lower the overall reduction strength ($M^{+/0}$ *vs* $T^{+/0*}$). Unlike other transformed species, the two $[Ir(df(CF_3)ppy)_2(H_3\text{-}N\text{^}N)]^0$ complexes exhibit excited state potentials ($T^{0*/-}$) above the estimated E^0 of TEA, which enables further ancillary ligand saturation as indicated by MS. The resulting $[Ir(df(CF_3)\text{-}ppy)_2(H_6\text{-}N\text{^}N)]^-$ species are more reductive, but their excited state potentials still do not exceed those of the group 3 complexes. Instead, the high oxidation strength of these complexes may allow reductive quenching with TEA, forming $[Ir(df(CF_3)ppy)_2(H_3\text{-}N\text{^}N)]^-$ and $[Ir(df(CF_3)ppy)_2(H_6\text{-}N\text{^}N)]^{2-}$, which exhibit potentials at approximately −1.5 V and −1.9 V *vs* SCE, respectively. Regardless, the combined results indicate that $[Ir(df(CF_3)ppy)_2(N\text{^}N)]^+$ complexes, commonly used as photoredox catalysts, are inherently more vulnerable to degradation under photochemical conditions.

Although difficulties in accurately measuring ground state potentials (Figure S19a) and excited state energy (Figure S21a) add a degree of uncertainty, our current estimate of the $[Ir(ppy)_2(dtb\text{-}H_3\text{-}bpy)]^{0*/-}$ excited state potential remains −1.7 V *vs* SCE.[16] Nevertheless, this catalytic system has successfully reduced substrates with peak potentials (E_p^{red}) well beyond this estimate, extending to −2.72 V *vs* SCE (*vide infra*),[16−18] for which several issues should be considered. First, although the often cited cathodic peak potentials (E_p^{red}) of substrates exhibiting irreversible electron transfer provide a relative measure of their susceptibility to reduction, they are not sufficiently accurate estimates of E^0 to evaluate reaction exergonicity.[64] Second, luminescence quenching experiments attempting to confirm PET between $[Ir(ppy)_2(dtb\text{-}H_3\text{-}bpy)]^0$ and a given substrate[16−18] are complicated by small remaining quantities of $[Ir(ppy)_2(dtb\text{-}bpy)]^+$ and the large excess of TEA (required for rapid *in situ* transformation). These species, and related amine photo-oxidation products, may lower the effective reduction potential of substrates through processes such as proton-coupled electron transfer and XAT (Figure 2b).[4,35] Moreover, the photoexcited transformed complex may be reductively quenched by species such as $[Ir(ppy)_2(dtb\text{-}bpy)]^0$ or the α-amino radical derived from the electron donor,

https://doi.org/10.1021/jacs.2c02011
J. Am. Chem. Soc. 2022, 144, 11189−11202

which would extend the catalyst reduction strength ($T^{0/-}$) to −1.97 V *vs* SCE, but this has not been experimentally verified. Finally, further spectroscopic interrogation is required to rule out alternative multiphoton pathways, such as con-PET, substrate sensitization, or electron expulsion.[22,47,48] The ability of this catalytic system to reduce substrates exhibiting peak potentials (E_p^{red}) that approach −3.0 V *vs* SCE likely involves a combination of the transformative side-reaction (Figure 2a) and at least one of the above factors.

High-Throughput Screening Recontextualized. We can extrapolate our findings from the detailed investigation of selected photocatalysts to the initial combinatorial screen. Most notably, analysis of $[Ir(ppy)_2(phen)]^+$ and the follow up high-throughput screening of intensely absorbing species confirms that complexes containing 1,10-phenanthroline derivatives (rows F−H) undergo PET to generate a reduced intermediate resistant to further side-reactions. Despite poor complexation of 2,2′-biquinoline to the cyclometalated iridium(III) core, the absorption data suggests these complexes form an intensely absorbing radical intermediate that is also resistant to chemical transformation. The relatively slower reduction of 4,7-dimethyl-1,10-phenanthroline complexes (row G, see Figure S12, Table S2) likely results from either a low Stern−Volmer quenching rate constant or a higher incidence of back electron transfer. Recent kinetic analysis of PET in iridium(III) complexes suggests charge recombination is affected by subtle differences in ligand environment and substitution.[46,65]

The screening revealed that photochemical transformation is widespread in complexes containing 2,2′-bipyridines (rows A−D), and MS analysis confirms similar saturation of the ancillary ligand by a HAT-capable sacrificial electron donor. The likelihood of either a blue- or red shift in emission can be rationalized by considering the effect of ligand saturation on the frontier orbitals. Partial saturation of the bipyridine ring system destabilizes both the ancillary ligand π^* orbitals (LUMO), by breaking aromaticity, as well as the metal t_{2g} orbitals (HOMO), due to increased electron donation from the anionic nitrogen. In complexes initially exhibiting type I excited states (^{3}MLLCT), the transformation changes the excited state morphology to type III/IV (dominant ^{3}LC character), and the large resulting blue shift represents the energy gap between the lowest lying π^* orbitals associated with the ancillary and cyclometalating ligands. In complexes that begin with type III/IV excited states, these unoccupied orbitals are more similar in energy.[50] Because the cyclometalating ligands (and therefore the associated ^{3}LC state) are less affected by the photochemical side-reaction, transformation in complexes with type III/IV excited states undergo greater relative HOMO destabilization, affording minimal change or a red shift in emission color. The slower color change observed for complexes containing 4,4′-diphenyl-2,2′-bipyridine (row D) and the greater persistence of their $[Ir(C^N)_2(N^N^{\bullet-})]^0$ intermediates (Figure S12, Table S2) further supports that increased conjugation stabilizes the radical and inhibits side-reactions. These complexes represent a midpoint between the photochemical reactivity of 2,2′-bipyridines and the stability of rigid 1,10-phenanthrolines and 2,2′-biquinolines.

Finally, the same analysis may rationalize the photochemical behavior of complexes classified as group 5, characterized by increasing emission intensity without changing color. Group 5 is strongly represented in complexes with type III/IV excited state morphologies (Figure 4f), where the lowest excited state is ^{3}LC in character. Transformation of the ancillary ligand is therefore unlikely to significantly affect emission properties. The subtle shifts in emission spectra measured for transformation of $[Ir(bt)_2(dm\text{-}bpy)]^+$ (in group 4 with type III/IV excited state)[50] support this hypothesis, and similar small changes in other complexes may not be detected by the photoreactor camera or discriminated by the plate sorting analysis.

Implications for Chemical Synthesis. The above experiments, focused on the scope of catalyst transformation and its effect on catalytic properties, were performed in the absence of organic substrates. In a synthetic photoredox reaction, electron transfer between reactive catalyst intermediates and the organic substrate can limit the formation of catalyst by-products.[14] Similarly, in this instance, substrates that react with either excited $[Ir(C^N)_2(N^N)]^{+*}$ or reduced $[Ir(C^N)_2(N^N)]^0$ intermediates may inhibit the transformation side-reaction. The differences in intermediate stability of $[Ir(C^N)_2(N^N)]^+$ complexes containing either 1,10-phenanthroline or 2,2′-bipyridine-type ancillary ligands (Figure 4) allow us to examine the competition between single- and multiphoton catalytic pathways in synthetic photoredox chemistry. Reductive dehalogenation of aryl halides is a useful model to probe the difference in photocatalytic ability of $[Ir(ppy)_2(dtb\text{-}bpy)]^+$ and $[Ir(ppy)_2(phen)]^+$ (Figure 8a) using three substrates with different reduction peak potentials: 4-bromo-2-fluorobenzonitrile (E_p^{red} = −1.76 V *vs* SCE; Figure S22a), methyl 4-chlorobenzoate (E_p^{red} = −1.98 V *vs* SCE; Figure S22b), and 4-bromoanisole (E_p^{red} = −2.72 V *vs* SCE; Figure S22c). Neither photoexcited catalyst reacts directly with these substrates, but both are quenched by TEA (Figure S23).

The $[Ir(ppy)_2(phen)]^+$ catalyst engaged 4-bromo-2-fluorobenzonitrile and to a lesser degree, methyl 4-chlorobenzoate (20% yield over 24 h), but it did not reduce the 4-bromoanisole substrate (Figure 8b−d; Table S4). Knowing that this catalyst is impervious to transformation (Figure 5), we ascribe this reactivity to a single-photon reductive quenching pathway and rationalize the apparent energy deficiency ($E^0(M^{+/0})$ = −1.36 V *vs* SCE) as discussed above.

Products formed considerably faster and in higher yields using the $[Ir(ppy)_2(dtb\text{-}bpy)]^+$ catalyst (Figure 8). This could be attributed to more efficient PET with TEA, but the catalysts exhibit similar bimolecular quenching constants (k_q): 1.03 × 10^8 and 0.94 × 10^8 M^{-1} s^{-1} for $[Ir(ppy)_2(dtb\text{-}bpy)]^+$ and $[Ir(ppy)_2(phen)]^+$, respectively (Figure S23, Table S5). To determine the reaction efficiency of the 4-bromo-2-fluorobenzonitrile and methyl 4-chlorobenzoate substrates with either the reduced $[Ir(ppy)_2(dtb\text{-}bpy^{\bullet-})]^0$ ($E^0(M^{+/0})$ = −1.46 V *vs* SCE) or transformed $[Ir(ppy)_2(dtb\text{-}H_3\text{-}bpy)]^0$ ($E^0(T^{+/0*})$ = −1.7 V *vs* SCE), we monitored the concentration of these species over the initial 20 min of reaction (Figures 9, S24). With the more difficult to reduce substrate (methyl 4-chlorobenzoate), the transient $[Ir(ppy)_2(dtb\text{-}bpy^{\bullet-})]^0$ accumulated rapidly (Figure 9a), but to a lesser extent than without substrate present, indicating some direct reaction with this intermediate. Nevertheless, within the first few minutes of the reaction, most of the catalyst transformed into $[Ir(ppy)_2(dtb\text{-}H_3\text{-}bpy)]^0$ (Figure 9b). In contrast, reaction of 4-bromo-2-fluorobenzonitrile exhibited a slower accumulation of reduced $[Ir(ppy)_2(dtb\text{-}bpy^{\bullet-})]^0$ and considerable inhibition of the catalyst transformation pathway (Figure 9). This resulted in a higher steady-state concentration of $[Ir(ppy)_2(dtb\text{-}bpy^{\bullet-})]^0$

https://doi.org/10.1021/jacs.2c02011
J. Am. Chem. Soc. 2022, 144, 11189−11202

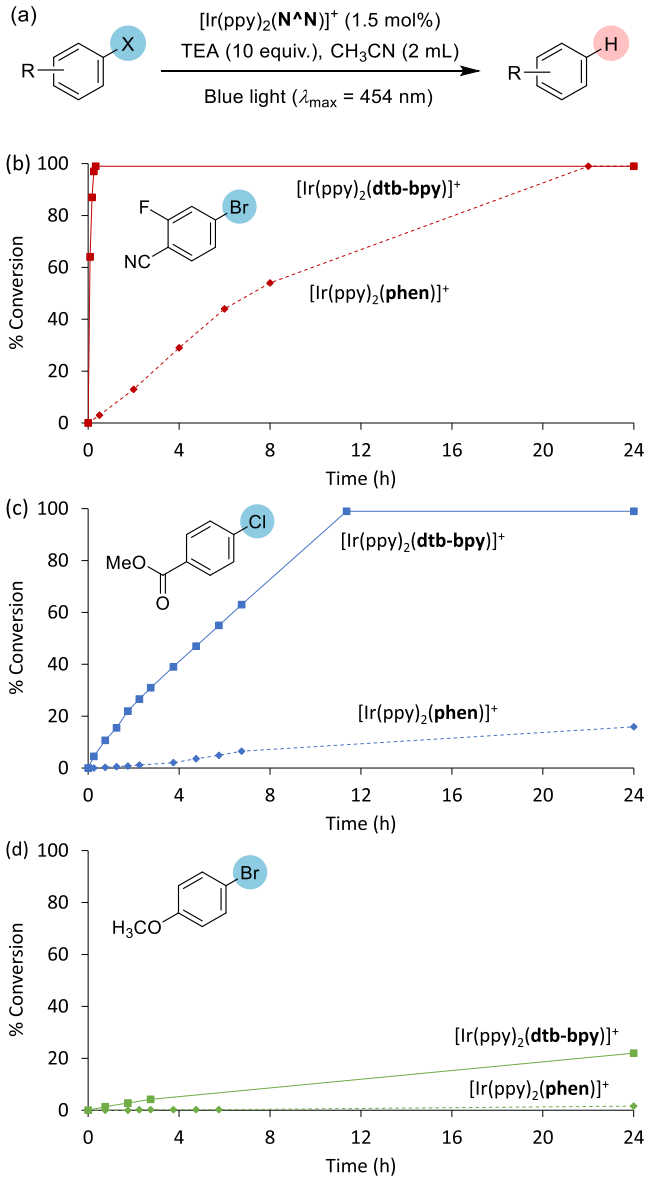

Figure 8. (a) Representative scheme for photocatalytic reductive dehalogenation of aryl halides, under blue light (two 5 W blue LEDs, λ_{max} = 454 nm). (b–d) Comparing the conversion, measured by HPLC, of (b) 4-bromo-2-fluorobenzonitrile, (c) methyl 4-chlorobenzoate, and (d) 4-bromoanisole (0.1 mmol; 50 mM) to their respective products over time using either $[Ir(ppy)_2(dtb\text{-}bpy)]^+$ (solid lines) or $[Ir(ppy)_2(phen)]^+$ (dashed lines). Note: a higher product yield for the 4-bromoanisole substrate with the $[Ir(ppy)_2(dtb\text{-}bpy)]^+$ catalyst was previously obtained[16] under more intense blue-light irradiation.

(greater turnover of the conventional reductive quenching photoredox cycle) and a low steady-state concentration of $[Ir(ppy)_2(dtb\text{-}H_3\text{-}bpy)]^0$.

While substrate reduction with $[Ir(ppy)_2(dtb\text{-}bpy^{\bullet-})]^0$ appears more efficient than with $[Ir(ppy)_2(phen^{\bullet-})]^0$, it is clear that catalyst transformation is a major pathway for $[Ir(ppy)_2(dtb\text{-}bpy)]^+$ under these conditions. Substrates that require more negative potentials for reduction will react less efficiently with $[Ir(ppy)_2(dtb\text{-}bpy^{\bullet-})]^0$, enabling greater transformation into $[Ir(ppy)_2(dtb\text{-}H_3\text{-}bpy)]^0$, which in turn enhances reaction efficiency through its greater reduction strength. It should be noted that our experiments do not

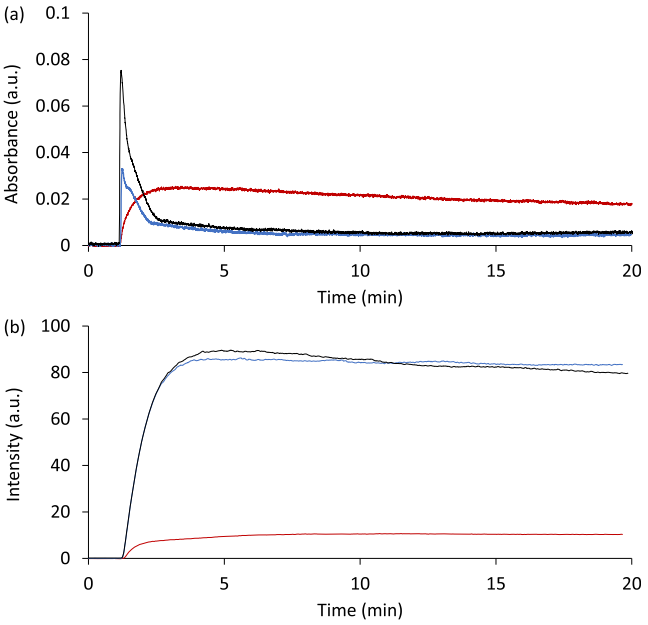

Figure 9. Monitoring (a) absorbance of the reduced $[Ir(ppy)_2(dtb\text{-}bpy^{\bullet-})]^0$ species (λ_{abs} = 533 nm) and (b) emission of the transformed $[Ir(ppy)_2(dtb\text{-}H_3\text{-}bpy)]^0$ catalyst (λ_{em} = 465 nm) during the reductive dehalogenation (0.2 mmol substrate; 6.6 mM) of 4-bromo-2-fluorobenzonitrile (red plots) and methyl 4-chlorobenzoate (blue plots), under blue-light irradiation with $[Ir(ppy)_2(dtb\text{-}bpy)]^+$ (3 mol %; 0.2 mM) and TEA (10 equiv.; 66 mM). Black plots represent the same experimental conditions in the absence of the substrate. Emission spectra before and after the 20 min irradiation time are shown in Figure S24.

account for possible differences in charge recombination of the $\{[Ir(C\text{^}N)_2(N\text{^}N^{\bullet-})]^0{:}TEA^{\bullet+}\}$ encounter complex formed immediately after PET. Efficient charge recombination limits overall reaction turnover and is affected by ligand substitution.[65−67]

CONCLUSIONS

Combining high-throughput screening and thorough characterization of select $[Ir(C\text{^}N)_2(N\text{^}N)]^+$ complexes allowed us to understand the links between stability and reactivity in the critical, reduced intermediate of a (reductive quenching) photoredox cycle. We found that this balance is primarily determined by ancillary ligand structure. Complexes with 1,10-phenanthroline derivatives form stable $[Ir(C\text{^}N)_2(N\text{^}N^{\bullet-})]^0$ species that resist further transformation. While this minimizes the likelihood of side-reactions, which could be advantageous for photochemical reactions, other studies have shown that these ancillary ligands generally cause poor catalytic performance due to enhanced charge recombination with sacrificial reductants.[65]

Conversely, partial saturation of 2,2′-bipyridine-type ancillary ligands is widespread when coupled with HAT-capable electron donors such as TEA and TEOA. The now anionic ligand (e.g., dtb-H_3-bpy$^-$) destabilizes both iridium (t_{2g}) and empty ligand ($\pi^*_{N\text{^}N}$) orbitals, thereby affording more negative ground and excited state potentials. In complexes where the lowest energy unoccupied orbitals associated with the ancillary and cyclometalating ligands are energetically different ($\pi^*_{C\text{^}N} \gg \pi^*_{N\text{^}N}$), such as $[Ir(ppy)_2(dtb\text{-}bpy)]^+$, transformation extends the reduction window of the photoredox system to at least −1.7 V *vs* SCE (compared to −1.47 V *vs* SCE) *via* a

https://doi.org/10.1021/jacs.2c02011
J. Am. Chem. Soc. 2022, 144, 11189−11202

tandem multiphoton mechanism. Complexes where the unoccupied orbitals are close in energy ($\pi^*_{C^N} \approx \pi^*_{N^N}$) provide no advantage from a multiphoton tandem photoredox mechanism. This is particularly notable in the common photooxidants $[Ir(df(CF_3)ppy)_2(bpy)]^+$ and $[Ir(df(CF_3)ppy)_2(dtb\text{-}bpy)]^+$; transformation decreases their oxidizing power, and their high oxidation potentials also render these catalysts especially vulnerable to further degradation. In other words, catalyst transformation will not always improve substrate engagement and may instead act as a deleterious side-reaction, dependent on the catalyst and desired application.

A comparison of two catalyst classes, represented by $[Ir(ppy)_2(phen)]^+$ and $[Ir(ppy)_2(dtb\text{-}bpy)]^+$, in a synthetic photoredox reaction revealed that transformation becomes increasingly competitive along with substrate energy requirements. While transformation maintains high product turnover beyond a single-photon cycle, careful examination of the interplay between the catalyst, sacrificial electron donor, and substrate is still required to properly assess the ability of these systems to reduce substrates exhibiting peak potentials (E_p) approaching −3.0 V *vs* SCE. Our results suggest that higher reactivity comes at the price of reduced stability, and balancing these competing properties is the critical challenge in designing next-generation catalysts tailored for increasing synthetic demands. These considerations are also crucial for catalyst recycling and reuse, which is necessary if synthetic photoredox chemistry is to mature from academic to industrial application.

EXPERIMENTAL SECTION

General. Reagents and solvents were purchased from commercial sources and used without further purification, unless otherwise stated. The heteroleptic iridium(III) complexes $[Ir(df(CF_3)ppy)_2(bpy)]PF_6$ and $[Ir(df(CF_3)ppy)_2(dtb\text{-}bpy)]PF_6$ were purchased from Oakwood Chemicals, and $[Ir(ppy)_2(dtb\text{-}bpy)]PF_6$ was purchased from Aldrich. All other iridium(III) complexes were prepared following previously published procedures.[51,56] The organic soluble bis(tetra-*n*-butylammonium) oxalate salt was prepared following a previously published procedure.[16] Acetonitrile was distilled over calcium hydride under a nitrogen atmosphere and collected as needed. ESI-MS experiments were performed using a Shimadzu LCMS-9030 quadrupole time-of-flight mass spectrometer. To obtain the mass spectra of complexes after photoinitiated transformation, the samples were prepared and the remaining TEA removed in the same manner used to measure the oxidation potential (*vide infra*), except that the dried complex was redissolved in neat acetonitrile. Tandem MS/MS experiments were performed by selecting the precursor ion and subjecting it to varying normalized collision energy between 30 and 70 eV in a higher-energy collisional dissociation (HCD) cell.

High-Throughput Parallel Synthesis and Screening. Reactions were performed using a 96-well plate of 1 mL glass vials sealed with a silicon film coated with Teflon.[49,50] Aliquots (100 μL) of 12 iridium dimers ($[Ir(C^N)_2Cl]_2$; 0.5 mM in DMSO) and eight ancillary ligands (N^N; 1.0 mM in DMSO) were combined, sealed, and heated at 150 °C for 16 h to produce a library of 96 heteroleptic iridium(III) complexes. After cooling the synthesis plate, the *in situ* prepared heteroleptic $[Ir(C^N)_2(N^N)]^+$ complexes (200 μL, 0.5 mM) were diluted with TEOA in DMSO (300 μL, final concentration of 50 mM). Vials were mixed by sonication for 5 min and moved to the photoreactor (Figure S1). The photoreactor was sealed and purged with Ar gas for 2 h, until an internal O_2 sensor maintained a constant zero reading. Reaction vials were irradiated from underneath using two 100 W blue LEDs (λ_{max} = 440−450 nm) and imaged using two 10 W ultraviolet (λ_{max} = 375 nm) or white (3000−3500 K) LEDs positioned above the vials. Images were captured by a camera positioned underneath the vials, between the two irradiation LEDs. The LEDs and camera were controlled by a Raspberry Pi computer. Reaction solutions were irradiated for 80 min, with photos captured every 30 s. Photos were processed and digitized using a custom Mathematica script that extracted the hue, saturation, and brightness (from HSB color space) of each well over time. Sorting analysis of the plate data was performed using a custom script built in Python 3 with NumPy and SciPy libraries. Briefly, the hue and brightness of each iridium(III) complex were compared with and without TEOA to determine if a reaction took place. Brightness at the beginning and end of the photoreaction was compared, and complexes that exhibited a significant decrease in the emission intensity (>35%) were classified as group 2. All remaining complexes, where emission increased over the course of the photoreaction, were then classified according to changes in emission color (blue shift, red shift, or no change).

Flow System. Using a peristaltic pump (Gilson Minipuls 3), solutions were aspirated at 3.5 mL min^{-1} from a photoreaction chamber (Figure S4a) and pumped through a two- and/or three-window flow-through quartz cuvette for absorbance and/or photoluminescence measurements using a Cary 300 Bio absorption spectrophotometer or a Cary Eclipse fluorescence spectrometer, respectively, before returning to the chamber. The solution in the photoreaction chamber was degassed by bubbling with N_2 gas and then irradiated with two 5 W blue LEDs (λ_{max} = 454 nm). The photoreactor was housed in a bespoke enclosure (Figure S4c), made from 250 to 520 nm filtering acrylic sheets (J Tech Photonics, USA), allowing visual inspection without exposing the viewer to the intense source light. Emission spectra were corrected for the variation in instrument sensitivity over the wavelength range of the measurements, using a correction factor established using a quartz halogen tungsten lamp of standard spectral irradiance. To collect absorption spectra of electrochemically reduced species, the photoreaction chamber was replaced by a bulk electrolysis chamber (BASi, USA) fitted with three electrodes (Figure S4b,d): a reticulated vitreous carbon working, a Pt wire counter in a fritted cell containing $TBAPF_6$ (0.1 M) in acetonitrile, and a "leakless" Ag/AgCl reference (eDAQ). Solutions were degassed for 10 min using N_2 gas. A potential of 0.1 V beyond the $E^{0\prime}$ of each complex was applied.

Low-Temperature Spectra. Steady-state low-temperature spectra were collected using a Cary Eclipse fluorescence spectrometer (5 nm bandpass, 1 nm interval) and an OptistatDN Variable Temperature Liquid Nitrogen Cryostat (Oxford Instruments) with a custom-made quartz sample holder.[68] Spectra were collected at 85 K to avoid damage to the sample holder near 77 K.[69,70] No difference was observed in λ_{max} at these two temperatures for complexes such as $[Ru(bpy)_3]^{2+}$ and $Ir(ppy)_3$ under our conditions (5 μM, 4:1 ethanol/methanol).[68] To collect low-temperature spectra after photochemical transformation, a solution of the complex (0.5 mM) and TEA (50 mM) in acetonitrile was degassed and irradiated in the photoreaction chamber. The solution was diluted 100-fold (5 μM) in 4:1 ethanol/methanol, and spectra were collected as described above. Spectra were corrected for the change in instrument sensitivity across the wavelength range.

Cyclic Voltammetry. A cylindrical glass electrochemical cell with a custom-built Teflon lid,[71] a glassy carbon working electrode (CH Instruments), a platinum wire counter electrode, and a "leakless" Ag/AgCl reference electrode (eDAQ) was housed in a Faraday cage. Potentials were applied using an Autolab PGSTAT204 potentiostat, referenced in situ to the ferrocenium/ferrocene ($Fc^{+/0}$) couple and converted to SCE using $Fc^{+/0}$ = +0.4 V.[72] Electrodes were cleaned prior to each experiment. The working electrode was polished using 0.05 μm alumina powder on a felt pad with deionized water. Complex solutions were prepared in freshly distilled acetonitrile (0.5 mM) with $TBAPF_6$ as the supporting electrolyte (0.1 M) and degassed with Ar gas for 5 min prior to analysis.

Two different approaches were required to measure the reduction potentials of photochemically transformed complexes. To determine the potential at which the complex is reduced ($T^{0/-}$), an acetonitrile solution of iridium(III) complex (0.5 mM), TEA (50 mM), and $TBAPF_6$ (0.1 M) was degassed with N_2 and cyclic voltammograms collected before and after irradiation with a 5 W blue LED (λ_{max} = 454 nm) mounted next to the cell. Under these conditions, the potential

https://doi.org/10.1021/jacs.2c02011
J. Am. Chem. Soc. 2022, 144, 11189−11202

range where the complex is oxidized ($T^{+/0}$) was obscured by the large excess of TEA (E^0 = 0.95 V *vs* SCE[58]). Instead, the complex (1 mM) and TEA (50 mM) in acetonitrile (4 mL) were degassed with N_2 gas for 10 min and then irradiated in the photochemical reaction chamber. The solution was diluted with dichloromethane (50 mL), then washed twice with acetic acid (0.1 M, 10 mL) and deionized water (10 mL) to remove excess TEA and reaction by-products. The remaining solution was then dried under vacuum and redissolved in acetonitrile with $TBAPF_6$ (0.1 M, 3 mL) and analyzed in the electrochemical cell.

Aryl Halide Reduction. The aryl halide substrate (0.1 mmol), TEA (1.0 mmol) and iridium(III) photocatalyst (1.5 mol %) were added to acetonitrile (2 mL) in a screw-cap glass vial. The reaction mixture was sealed with a septum lid and sparged with N_2 for 10 min. Reactions were irradiated in the photoreaction chamber with two 5 W blue LEDs (λ_{max} = 454 nm) for 24 h. Samples (10 μL) were periodically collected and diluted with 1 mL solvent (30% acetonitrile, 70% deionized water) prior to chromatographic analysis. Reverse-phase HPLC was performed using an Agilent 1260 Infinity system with a quaternary pump. An aliquot (10 μL) of the diluted sample was injected onto a Poroshell 120 EC-C18 4.6 × 50 mm column (2 μm), with a linear gradient from 30 to 100% acetonitrile over 8 min at 25 °C. Each run was followed by 5 min re-equilibration time. UV absorption detection was set at 227 nm. Calibration curves were prepared using either substrate or product standards.

■ ASSOCIATED CONTENT

Supporting Information

The Supporting Information is available free of charge at https://pubs.acs.org/doi/10.1021/jacs.2c02011.

Description of high-throughput equipment; extra experimental data; and photos of changing emission color (PDF)

■ AUTHOR INFORMATION

Corresponding Authors

Paul S. Francis − *School of Life and Environmental Sciences, Deakin University, Geelong, Victoria 3220, Australia*; Email: paul.francis@deakin.edu.au

Stefan Bernhard − *Department of Chemistry, Carnegie Mellon University, Pittsburgh, Pennsylvania 15213, United States*; orcid.org/0000-0002-8033-1453; Email: bern@cmu.edu

Timothy U. Connell − *School of Life and Environmental Sciences, Deakin University, Geelong, Victoria 3220, Australia*; orcid.org/0000-0002-6142-3854; Email: t.connell@deakin.edu.au

Authors

Joseph C. Bawden − *School of Life and Environmental Sciences, Deakin University, Geelong, Victoria 3220, Australia*

Stephen DiLuzio − *Department of Chemistry, Carnegie Mellon University, Pittsburgh, Pennsylvania 15213, United States*

David J. Hayne − *Institute for Frontier Materials, Deakin University, Geelong, Victoria 3220, Australia*; orcid.org/0000-0003-2756-9427

Egan H. Doeven − *School of Life and Environmental Sciences, Deakin University, Geelong, Victoria 3220, Australia*

Johnny Truong − *School of Science, RMIT University, Melbourne, Victoria 3000, Australia*

Richard Alexander − *Centre for Regional and Rural Futures, Deakin University, Geelong, Victoria 3220, Australia*; orcid.org/0000-0001-6121-7885

Luke C. Henderson − *Institute for Frontier Materials, Deakin University, Geelong, Victoria 3220, Australia*; orcid.org/0000-0002-4244-2056

Daniel E. Gómez − *School of Science, RMIT University, Melbourne, Victoria 3000, Australia*; orcid.org/0000-0002-7871-4068

Massimiliano Massi − *School of Molecular and Life Sciences, Curtin University, Bentley, Western Australia 6102, Australia*; orcid.org/0000-0001-6949-4019

Blake I. Armstrong − *School of Molecular and Life Sciences, Curtin University, Bentley, Western Australia 6102, Australia*

Felicity A. Draper − *School of Life and Environmental Sciences, Deakin University, Geelong, Victoria 3220, Australia*

Complete contact information is available at: https://pubs.acs.org/10.1021/jacs.2c02011

Notes

The authors declare no competing financial interest.

■ ACKNOWLEDGMENTS

The authors thank the Australian Research Council (DP200102947; DE210101168; and DP220100300) for funding this work, Leslie Gamel (The University of Melbourne) for the construction of quartz sample holders used to collect low temperature spectra, and Dr Lawrence Webb and Dr Jacqui Adcock (Deakin University) for their assistance in mass spectrometry and HPLC experiments.

■ REFERENCES

(1) Glaser, F.; Wenger, O. S. Recent progress in the development of transition-metal based photoredox catalysts. *Coord. Chem. Rev.* **2020**, *405*, 213129.

(2) Cybularczyk-Cecotka, M.; Szczepanik, J.; Giedyk, M. Photocatalytic strategies for the activation of organic chlorides. *Nat. Catal.* **2020**, *3*, 872−886.

(3) Cannalire, R.; Pelliccia, S.; Sancineto, L.; Novellino, E.; Tron, G. C.; Giustiniano, M. Visible light photocatalysis in the late-stage functionalization of pharmaceutically relevant compounds. *Chem. Soc. Rev.* **2021**, *50*, 766−897.

(4) Murray, P. R. D.; Cox, J. H.; Chiappini, N. D.; Roos, C. B.; McLoughlin, E. A.; Hejna, B. G.; Nguyen, S. T.; Ripberger, H. H.; Ganley, J. M.; Tsui, E.; Shin, N. Y.; Koronkiewicz, B.; Qiu, G.; Knowles, R. R. Photochemical and Electrochemical Applications of Proton-Coupled Electron Transfer in Organic Synthesis. *Chem. Rev.* **2022**, *122*, 2017−2291.

(5) Tay, N. E. S.; Lehnherr, D.; Rovis, T. Photons or Electrons? A Critical Comparison of Electrochemistry and Photoredox Catalysis for Organic Synthesis. *Chem. Rev.* **2022**, *122*, 2487−2649.

(6) Reed, N. L.; Yoon, T. P. Oxidase reactions in photoredox catalysis. *Chem. Soc. Rev.* **2021**, *50*, 2954−2967.

(7) Pitre, S. P.; Overman, L. E. Strategic Use of Visible-Light Photoredox Catalysis in Natural Product Synthesis. *Chem. Rev.* **2022**, *122*, 1717−1751.

(8) Vaidyalingam, A.; Dutta, P. K. Analysis of the Photodecomposition Products of $Ru(bpy)_3^{2+}$ in Various Buffers and upon Zeolite Encapsulation. *Anal. Chem.* **2000**, *72*, 5219−5224.

(9) Khnayzer, R. S.; Thoi, V. S.; Nippe, M.; King, A. E.; Jurss, J. W.; El Roz, K. A.; Long, J. R.; Chang, C. J.; Castellano, F. N. Towards a comprehensive understanding of visible-light photogeneration of hydrogen from water using cobalt(II) polypyridyl catalysts. *Energy Environ. Sci.* **2014**, *7*, 1477−1488.

(10) Tinker, L. L.; McDaniel, N. D.; Curtin, P. N.; Smith, C. K.; Ireland, M. J.; Bernhard, S. Visible light induced catalytic water

reduction without an electron relay. *Chem. Eur. J.* **2007**, *13*, 8726−8732.
(11) Devery, J. J., III; Douglas, J. J.; Nguyen, J. D.; Cole, K. P.; Flowers, R. A.; Stephenson, C. R. J. Ligand functionalization as a deactivation pathway in a fac-Ir(ppy)$_3$-mediated radical addition. *Chem. Sci.* **2015**, *6*, 537−541.
(12) Stephenson, C.; Swift, E.; Williams, T. Intermolecular photocatalytic C−H functionalization of electron-rich heterocycles with tertiary alkyl halides. *Synlett* **2016**, *27*, 754−758.
(13) Peng, H.-L.; Li, Y.; Chen, X.-Y.; Li, L.-P.; Ke, Z.; Ye, B.-H. Visible-light-induced amination of quinoline at the C8 position via a postcoordinated interligand-coupling strategy under mild conditions. *Inorg. Chem.* **2021**, *60*, 908−918.
(14) Schmid, L.; Glaser, F.; Schaer, R.; Wenger, O. S. High Triplet Energy Iridium(III) Isocyanoborato Complex for Photochemical Upconversion, Photoredox and Energy Transfer Catalysis. *J. Am. Chem. Soc.* **2022**, *144*, 963−976.
(15) Grotjahn, S.; König, B. Photosubstitution in Dicyanobenzene-based Photocatalysts. *Org. Lett.* **2021**, *23*, 3146−3150.
(16) Connell, T. U.; Fraser, C. L.; Czyz, M. L.; Smith, Z. M.; Hayne, D. J.; Doeven, E. H.; Agugiaro, J.; Wilson, D. J. D.; Adcock, J. L.; Scully, A. D.; Gómez, D. E.; Barnett, N. W.; Polyzos, A.; Francis, P. S. The Tandem Photoredox Catalysis Mechanism of $[Ir(ppy)_2(dtb\text{-}bpy)]^+$ Enabling Access to Energy Demanding Organic Substrates. *J. Am. Chem. Soc.* **2019**, *141*, 17646−17658.
(17) Forni, J. A.; Micic, N.; Connell, T. U.; Weragoda, G.; Polyzos, A. Tandem Photoredox Catalysis: Enabling Carbonylative Amidation of Aryl and Alkylhalides. *Angew. Chem., Int. Ed.* **2020**, *59*, 18646−18654.
(18) Czyz, M. L.; Taylor, M. S.; Horngren, T. H.; Polyzos, A. Reductive activation and hydrofunctionalization of olefins by multiphoton tandem photoredox catalysis. *ACS Catal.* **2021**, *11*, 5472−5480.
(19) MacKenzie, I. A.; Wang, L.; Onuska, N. P. R.; Williams, O. F.; Begam, K.; Moran, A. M.; Dunietz, B. D.; Nicewicz, D. A. Discovery and characterization of an acridine radical photoreductant. *Nature* **2020**, *580*, 76−80.
(20) Targos, K.; Williams, O. P.; Wickens, Z. K. Unveiling Potent Photooxidation Behavior of Catalytic Photoreductants. *J. Am. Chem. Soc.* **2021**, *143*, 4125−4132.
(21) Xu, J.; Cao, J.; Wu, X.; Wang, H.; Yang, X.; Tang, X.; Toh, R. W.; Zhou, R.; Yeow, E. K. L.; Wu, J. Unveiling Extreme Photoreduction Potentials of Donor-Acceptor Cyanoarenes to Access Aryl Radicals from Aryl Chlorides. *J. Am. Chem. Soc.* **2021**, *143*, 13266−13273.
(22) Kerzig, C.; Guo, X.; Wenger, O. S. Unexpected hydrated electron source for preparative visible-light driven photoredox catalysis. *J. Am. Chem. Soc.* **2019**, *141*, 2122−2127.
(23) Kerzig, C.; Wenger, O. S. Reactivity control of a photocatalytic system by changing the light intensity. *Chem. Sci.* **2019**, *10*, 11023−11029.
(24) Glaser, F.; Kerzig, C.; Wenger, O. S. Multi-Photon Excitation in Photoredox Catalysis: Concepts, Applications, Methods. *Angew. Chem., Int. Ed.* **2020**, *59*, 10266−10284.
(25) Pfund, B.; Steffen, D. M.; Schreier, M. R.; Bertrams, M.-S.; Ye, C.; Börjesson, K.; Wenger, O. S.; Kerzig, C. UV light generation and challenging photoreactions enabled by upconversion in water. *J. Am. Chem. Soc.* **2020**, *142*, 10468−10476.
(26) Glaser, F.; Kerzig, C.; Wenger, O. S. Sensitization-initiated electron transfer via upconversion: mechanism and photocatalytic applications. *Chem. Sci.* **2021**, *12*, 9922−9933.
(27) Chatterjee, A.; König, B. Birch-Type Photoreduction of Arenes and Heteroarenes by Sensitized Electron Transfer. *Angew. Chem., Int. Ed.* **2019**, *58*, 14289−14294.
(28) Hayne, D. J.; Mohapatra, S.; Bawden, J. C.; Adcock, J. L.; Barbante, G. J.; Doeven, E. H.; Fraser, C. L.; Connell, T. U.; White, J. M.; Henderson, L. C.; Francis, P. S. Catalyst luminescence exploited as an inherent in situ probe of photoredox catalysis. *ChemPhotoChem* **2020**, *4*, 105−109.
(29) Coles, M. S.; Quach, G.; Beves, J. E.; Moore, E. G. A Photophysical Study of Sensitization-Initiated Electron Transfer: Insights into the Mechanism of Photoredox Activity. *Angew. Chem., Int. Ed.* **2020**, *59*, 9522−9526.
(30) Naumann, R.; Kerzig, C.; Goez, M. Laboratory-scale photoredox catalysis using hydrated electrons sustainably generated with a single green laser. *Chem. Sci.* **2017**, *8*, 7510−7520.
(31) Nakajima, M.; Fava, E.; Loescher, S.; Jiang, Z.; Rueping, M. Photoredox-catalyzed reductive coupling of aldehydes, ketones, and imines with visible light. *Angew. Chem., Int. Ed.* **2015**, *54*, 8828−8832.
(32) Kim, S.; Park, G.; Cho, E. J.; You, Y. Coreactant strategy for the photoredox catalytic generation of trifluoromethyl radicals under low-energy photoirradiation. *J. Org. Chem.* **2016**, *81*, 7072−7079.
(33) Shen, Y.; Cornella, J.; Juliá-Hernández, F.; Martin, R. Visible-light-promoted atom transfer radical cyclization of unactivated alkyl iodides. *ACS Catal.* **2017**, *7*, 409−412.
(34) Guo, X.; Wenger, O. S. Reductive Amination by Photoredox Catalysis and Polarity-Matched Hydrogen Atom Transfer. *Angew. Chem., Int. Ed.* **2018**, *57*, 2469−2473.
(35) Constantin, T.; Zanini, M.; Regni, A.; Sheikh, N. S.; Juliá, F.; Leonori, D. Aminoalkyl radicals as halogen-atom transfer agents for activation of alkyl and aryl halides. *Science* **2020**, *367*, 1021−1026.
(36) Constantin, T.; Juliá, F.; Sheikh, N. S.; Leonori, D. A case of chain propagation: α-aminoalkyl radicals as initiators for aryl radical chemistry. *Chem. Sci.* **2020**, *11*, 12822−12828.
(37) Chmiel, A. F.; Williams, O. P.; Chernowsky, C. P.; Yeung, C. S.; Wickens, Z. K. Non-innocent radical ion intermediates in photoredox catalysis: parallel reduction modes enable coupling of diverse aryl chlorides. *J. Am. Chem. Soc.* **2021**, *143*, 10882−10889.
(38) Yue, F.; Dong, J.; Liu, Y.; Wang, Q. Visible-Light-Mediated C-I Difluoroallylation with an α-Aminoalkyl Radical as a Mediator. *Org. Lett.* **2021**, *23*, 7306−7310.
(39) Hu, J.; Wang, J.; Nguyen, T. H.; Zheng, N. The chemistry of amine radical cations produced by visible light photoredox catalysis. *Beilstein J. Org. Chem.* **2013**, *9*, 1977−2001.
(40) Beatty, J. W.; Stephenson, C. R. J. Amine functionalization via oxidative photoredox catalysis: methodology development and complex molecule synthesis. *Acc. Chem. Res.* **2015**, *48*, 1474−1484.
(41) Ghosh, I.; Bardagi, J. I.; König, B. Reply to "Photoredox Catalysis: The Need to Elucidate the Photochemical Mechanism". *Angew. Chem., Int. Ed.* **2017**, *56*, 12822−12824.
(42) Ghosh, I.; Shaikh, R. S.; König, B. Sensitization-Initiated Electron Transfer for Photoredox Catalysis. *Angew. Chem., Int. Ed.* **2017**, *56*, 8544−8549.
(43) Marchini, M.; Bergamini, G.; Cozzi, P. G.; Ceroni, P.; Balzani, V. Photoredox Catalysis: The Need to Elucidate the Photochemical Mechanism. *Angew. Chem., Int. Ed.* **2017**, *56*, 12820−12821.
(44) Marchini, M.; Gualandi, A.; Mengozzi, L.; Franchi, P.; Lucarini, M.; Cozzi, P. G.; Balzani, V.; Ceroni, P. Mechanistic insights into two-photon-driven photocatalysis in organic synthesis. *Phys. Chem. Chem. Phys.* **2018**, *20*, 8071−8076.
(45) Chernowsky, C. P.; Chmiel, A. F.; Wickens, Z. K. Electrochemical Activation of Diverse Conventional Photoredox Catalysts Induces Potent Photoreductant Activity. *Angew. Chem., Int. Ed.* **2021**, *60*, 21418−21425.
(46) Aydogan, A.; Bangle, R. E.; De Kreijger, S.; Dickenson, J. C.; Singleton, M. L.; Cauët, E.; Cadranel, A.; Meyer, G. J.; Elias, B.; Sampaio, R. N.; Troian-Gautier, L. Mechanistic investigation of a visible light mediated dehalogenation/cyclisation reaction using iron(III), iridium(III) and ruthenium(II) photosensitizers. *Catal. Sci. Technol.* **2021**, *11*, 8037−8051.
(47) Giedyk, M.; Narobe, R.; Weiß, S.; Touraud, D.; Kunz, W.; König, B. Photocatalytic activation of alkyl chlorides by assembly-promoted single electron transfer in microheterogeneous solutions. *Nat. Catal.* **2020**, *3*, 40−47.
(48) Santos, M. S.; Cybularczyk-Cecotka, M.; König, B.; Giedyk, M. Minisci C−H Alkylation of Heteroarenes Enabled by Dual Photoredox/Bromide Catalysis in Micellar Solutions**. *Chem. Eur. J.* **2020**, *26*, 15323−15329.

https://doi.org/10.1021/jacs.2c02011
J. Am. Chem. Soc. 2022, 144, 11189−11202

(49) Mdluli, V.; Diluzio, S.; Lewis, J.; Kowalewski, J. F.; Connell, T. U.; Yaron, D.; Kowalewski, T.; Bernhard, S. High-throughput synthesis and screening of iridium(III) photocatalysts for the fast and chemoselective dehalogenation of aryl bromides. *ACS Catal.* **2020**, *10*, 6977−6987.
(50) DiLuzio, S.; Mdluli, V.; Connell, T. U.; Lewis, J.; VanBenschoten, V.; Bernhard, S. High-throughput screening and automated data-driven analysis of the triplet photophysical properties of structurally diverse, heteroleptic iridium(III) complexes. *J. Am. Chem. Soc.* **2021**, *143*, 1179−1194.
(51) Lowry, M. S.; Goldsmith, J. I.; Slinker, J. D.; Rohl, R.; Pascal, R. A., Jr.; Malliaras, G. G.; Bernhard, S. Single-layer electroluminescent devices and photoinduced hydrogen production from an ionic iridium(III) complex. *Chem. Mater.* **2005**, *17*, 5712−5719.
(52) Ladouceur, S.; Fortin, D.; Zysman-Colman, E. Enhanced luminescent iridium(III) complexes bearing aryltriazole cyclometallated ligands. *Inorg. Chem.* **2011**, *50*, 11514−11526.
(53) Wu, S.-H.; Ling, J.-W.; Lai, S.-H.; Huang, M.-J.; Cheng, C. H.; Chen, I.-C. Dynamics of the Excited States of $[Ir(ppy)_2bpy]^+$ with Triple Phosphorescence. *J. Phys. Chem. A* **2010**, *114*, 10339−10344.
(54) Alrawashdeh, L. R.; Cronin, M. P.; Woodward, C. E.; Day, A. I.; Wallace, L. Iridium cyclometalated complexes in host-guest chemistry: a strategy for maximizing quantum yield in aqueous media. *Inorg. Chem.* **2016**, *55*, 6759−6769.
(55) Yen, H.-Y.; Huang, M.-J.; Chen, I.-C. Physical properties of triplet excited states of $[Ir(ppy)_2bpy]^+$ in polar solvent and in nonaqueous confined reversed micelle. *J. Photochem. Photobiol., A* **2016**, *318*, 33−41.
(56) Chen, L.; Hayne, D. J.; Doeven, E. H.; Agugiaro, J.; Wilson, D. J. D.; Henderson, L. C.; Connell, T. U.; Nai, Y. H.; Alexander, R.; Carrara, S.; Hogan, C. F.; Donnelly, P. S.; Francis, P. S. A conceptual framework for the development of iridium(III) complex-based electrogenerated chemiluminescence labels. *Chem. Sci.* **2019**, *10*, 8654−8667.
(57) Newman, B.; Chen, L.; Henderson, L. C.; Doeven, E. H.; Francis, P. S.; Hayne, D. J. Water-soluble iridium(III) complexes containing tetraethylene-glycol-derivatized bipyridine ligands for electrogenerated chemiluminescence detection. *Front. Chem.* **2020**, *8*, 583631.
(58) Kanoufi, F.; Zu, Y.; Bard, A. J. Homogeneous Oxidation of Trialkylamines by Metal Complexes and Its Impact on Electrogenerated Chemiluminescence in the Trialkylamine/$Ru(bpy)_3^{2+}$ System. *J. Phys. Chem. B* **2001**, *105*, 210−216.
(59) Isse, A. A.; Gennaro, A.; Maran, F.; Frölich, R.; Sillesen, A.; Mønsted, O.; Rasmussen, J. C.; Toftlund, H. Mechanism of the dissociative electro-oxidation of oxalate in aprotic solvents. *Acta Chem. Scand.* **1999**, *53*, 1013−1022.
(60) Huang, Y.; Hou, J.; Zhan, L.-W.; Zhang, Q.; Tang, W.-Y.; Li, B.-D. Photoredox activation of formate salts: hydrocarboxylation of alkenes via carboxyl group transfer. *ACS Catal.* **2021**, *11*, 15004−15012.
(61) Goldsmith, J. I.; Hudson, W. R.; Lowry, M. S.; Anderson, T. H.; Bernhard, S. Discovery and high-throughput screening of heteroleptic iridium complexes for photoinduced hydrogen production. *J. Am. Chem. Soc.* **2005**, *127*, 7502−7510.
(62) Zanoni, K. P. S.; Kariyazaki, B. K.; Ito, A.; Brennaman, M. K.; Meyer, T. J.; Murakami Iha, N. Y. Blue-green iridium(III) emitter and comprehensive photophysical elucidation of heteroleptic cyclometalated iridium(III) complexes. *Inorg. Chem.* **2014**, *53*, 4089−4099.
(63) Ener, M. E.; Darcy, J. W.; Menges, F. S.; Mayer, J. M. Base-Directed Photoredox Activation of C-H Bonds by PCET. *J. Org. Chem.* **2020**, *85*, 7175−7180.
(64) Espinoza, E. M.; Clark, J. A.; Soliman, J.; Derr, J. B.; Morales, M.; Vullev, V. I. Practical aspects of cyclic voltammetry: how to estimate reduction potentials when irreversibility prevails. *J. Electrochem. Soc.* **2019**, *166*, H3175−H3187.
(65) DiLuzio, S.; Connell, T. U.; Mdluli, V.; Kowalewski, J. F.; Bernhard, S. Understanding Ir(III) Photocatalyst Structure-Activity Relationships: A Highly Parallelized Study of Light-Driven Metal Reduction Processes. *J. Am. Chem. Soc.* **2022**, *144*, 1431−1444.
(66) Qin, Y.; Zhu, Q.; Sun, R.; Ganley, J. M.; Knowles, R. R.; Nocera, D. G. Mechanistic Investigation and Optimization of Photoredox Anti-Markovnikov Hydroamination. *J. Am. Chem. Soc.* **2021**, *143*, 10232−10242.
(67) Aydogan, A.; Bangle, R. E.; Cadranel, A.; Turlington, M. D.; Conroy, D. T.; Cauët, E.; Singleton, M. L.; Meyer, G. J.; Sampaio, R. N.; Elias, B.; Troian-Gautier, L. Accessing Photoredox Transformations with an Iron(III) Photosensitizer and Green Light. *J. Am. Chem. Soc.* **2021**, *143*, 15661−15673.
(68) Soulsby, L. C.; Hayne, D. J.; Doeven, E. H.; Wilson, D. J. D.; Agugiaro, J.; Connell, T. U.; Chen, L.; Hogan, C. F.; Kerr, E.; Adcock, J. L.; Donnelly, P. S.; White, J. M.; Francis, P. S. Mixed annihilation electrogenerated chemiluminescence of iridium(III) complexes. *Phys. Chem. Chem. Phys.* **2018**, *20*, 18995−19006.
(69) Mallet, C.; Bolduc, A.; Bishop, S.; Gautier, Y.; Skene, W. G. Unusually high fluorescence quantum yield of a homopolyfluorenylazomethine - towards a universal fluorophore. *Phys. Chem. Chem. Phys.* **2014**, *16*, 24382−24390.
(70) Chen, L.; Doeven, E. H.; Wilson, D. J. D.; Kerr, E.; Hayne, D. J.; Hogan, C. F.; Yang, W.; Pham, T. T.; Francis, P. S. Co-reactant Electrogenerated Chemiluminescence of Iridium(III) Complexes Containing an Acetylacetonate Ligand. *ChemElectroChem* **2017**, *4*, 1797−1808.
(71) Kerr, E.; Doeven, E. H.; Barbante, G. J.; Hogan, C. F.; Hayne, D. J.; Donnelly, P. S.; Francis, P. S. New perspectives on the annihilation electrogenerated chemiluminescence of mixed metal complexes in solution. *Chem. Sci.* **2016**, *7*, 5271−5279.
(72) Connelly, N. G.; Geiger, W. E. Chemical redox agents for organometallic chemistry. *Chem. Rev.* **1996**, *96*, 877−910.

https://doi.org/10.1021/jacs.2c02011
J. Am. Chem. Soc. 2022, 144, 11189−11202